

# **O and H isotopic evidence for a mantle source of water in appinite magma: an example from the Late Neoproterozoic Greendale Complex, Nova Scotia**

Ian P Cawood<sup>a</sup>, J Brendan Murphy<sup>b</sup>, William J McCarthy<sup>c</sup>, Adrian J Boyce<sup>d</sup>

*<sup>a</sup>Department of Earth Sciences, University of Oxford, OX1 3AN, UK*

*<sup>b</sup>Department of Earth Sciences, St Francis Xavier University, NS B2G 2W5, Canada*

*<sup>c</sup>School of Earth and Environmental Sciences, University of St Andrews, KY16 9AL, UK*

*<sup>d</sup>Scottish Universities Environmental Research Centre, G75 0QF, UK*

---

## **ABSTRACT**

Appinite suite rocks occur as small plutonic bodies, ranging from ultramafic to felsic in composition, that are characterized by abundant idiomorphic amphibole suggesting they are the products of water-rich mafic magmas. Appinites are also understood to record tectono-magmatic processes during the waning stages of subduction in convergent to collisional tectonic settings. Measuring D/H and  $^{18}\text{O}/^{16}\text{O}$  ratios of hornblende in appinitic rocks offers opportunities to constrain the sources of water (mantle, crustal, sea water and or meteoric) in the magma during its crystallization, and to shed light on the role of water as arc magmatism shuts down. The ca. 607 Ma Greendale Complex in the Avalon terrane of Nova Scotia, Canada, is characterized by spectacular exposures of appinite suite rocks ranging from ultramafic to felsic in composition. Two populations of amphiboles are identified: one is characterized by  $\delta^{18}\text{O}$  values between 4.7–

6.8 ‰ and anomalously low  $\delta D$  values (ca.  $< -90$  ‰). These isotopic signatures are interpreted to represent incorporation of mantle-derived fluids into the crystal structure, possibly associated with mixing between a region of mantle upwelling and a subducting slab. This mixing process allows for hydration of the magma during its ascent into the overlying lithospheric mantle wedge. Some amphiboles retain mantle-like  $\delta^{18}O$  and  $\delta D$  values, but others may have partially re-equilibrated during low T assimilation of supracrustal units (e.g. organic-rich sediments) and or fluids derived from such bodies. A second generation of hornblende yields  $\delta^{18}O$  varying from 0.9 to 4.6 ‰ and  $\delta D$  from ca.  $-106$  to  $-64$  ‰, which supports equilibration with fluids from crustal sources. Assimilation of volatiles sourced from previously hydrothermally altered intruded sheets and or country rock is interpreted to produce these second-generation isotopic signatures. Regional syntheses indicate that arc magmatism in the Avalon terrane ended with the generation of a transform system, implying the potential generation of a slab window behind that system. In that context, the Appinites in the Avalon terrane have previously been interpreted to have been emplaced after the cessation of subduction in a slab window or slab failure setting behind the transform system, in which asthenospheric upwelling generated juvenile magmas and/or facilitated melting of the overlying continental lithospheric mantle. Our  $\delta D$  and  $\delta^{18}O$  data support this model and together with available Sm-Nd data, suggest asthenospheric upwelling triggered melting of the continental lithospheric mantle that was previously hydrated by subduction and this mantle-derived water contributed to the origin of appinites.

## **1. Introduction**

Appinitic suite rocks occur in relatively small plutonic complexes typically around the periphery of voluminous granitoid batholiths (Atherton and Ghani, 2002; Bea et al., 1999; Castro

et al., 2003; Fowler, 1988; Fowler et al., 2001; Murphy, 2013, 2020; Pitcher, 1997; Pitcher and Berger, 1972). They are characterized by abundant idiomorphic amphibole, relative to olivine and pyroxene, in rocks of mafic and ultramafic composition which, together with the widespread development of mafic “pegmatites”, indicate that precursor magmas were anomalously water-rich (e.g. Bowes and McArthur, 1976; Murphy, 2013, 2020; Pitcher and Berger, 1972; Pitcher and Hutton, 2003). This interpretation is supported by a plethora of experimental studies which shows that at high  $pH_2O$  the stability field of amphibole expands relative to olivine, pyroxene, and plagioclase (Moore and Carmichael, 1998; Müntener et al., 2001). However, the source(s) of this water in appinites has never been directly investigated.

Appinites have a geochemical signature indicative of calc alkaline to shoshonitic affinities (e.g. Atherton and Ghani, 2002; Castro et al., 2003; Fowler, 1988). Their distinctive geochemistry has led to hypotheses postulating genetic relationships with high-Mg basalts (Tiepolo et al., 2011), shoshonitic lamprophyres (Rock, 1990), adakites (Ye et al., 2008), and sanukitoid and tonalite-trondhjemite-granodiorite (TTG) suites (Wilkin and Bornhorst, 1993). Sanukitoids have been postulated as markers of the beginning of post-Archean-style subduction (Fowler and Rollinson, 2012). Many studies also propose a genetic relationship between appinite complexes and granitoid batholiths (e.g. Bowes and McArthur, 1976; Fowler, 1988; Pitcher, 1997). Recent syntheses suggest that appinite suite rocks may preserve evidence of mantle processes that produce voluminous granitoid batholiths (Murphy, 2020) implying that understanding the source of the water from which they crystallize may also constrain models for granitoid magma genesis thus providing insight on the generation of continental crust (Collins et al., 2020).

Appinites are spatially associated with deep crustal faults and geodynamic processes associated with the cessation of subduction, such as post-subduction slab-break off, slab window generation and slab delamination during the latest stages of an orogeny (Atherton and Ghani, 2002; Castro et al., 2003; Murphy, 2013, 2020; Murphy and Hynes, 1990; Ye et al., 2008). Given the important role of water genesis in the production of arc magmas, the origin of water in appinite complexes has the potential to shed light on processes operating as subduction shuts down.

In this study, we focus on the late Neoproterozoic Greendale Complex, a spectacularly exposed body of appinite suite rocks in the Avalon terrane of northern Nova Scotia. We provide oxygen and hydrogen isotopic data on hornblende in various lithologies in this complex to constrain the sources of the water that resulted in hornblende crystallization. Our data identify an important component of mantle-derived water, which has implications for the origin of magmas in the waning stages of arc magmatism.

## **2. Geological setting and field relationships**

The late Neoproterozoic ( $607 \pm 2$  Ma, U-Pb titanite) Greendale Complex is a local representative of subduction-related magmatism that characterizes the Avalon terrane in the Canadian Appalachians (Murphy et al., 1997a). This magmatic activity occurred when Avalonia was located along the northern Gondwanan margin prior to its Late Cambrian-Early Ordovician separation from Gondwana and Late Silurian-Early Devonian accretion to Laurentia (Fig. 1a; Murphy et al., 1997b). The Greendale Complex occurs between two faults, the Hollow and

Greendale faults, which were active at the time of its emplacement (Fig. 1b, c; Murphy and Hynes, 1990). The complex intrudes the Chisholm Brook Formation (dominated by basalt with minor limestone) and the Morar Brook Formation (dominated black organic mudstone and siltstone, with minor limestone and chert) of the late Neoproterozoic Georgeville Group, a polydeformed arc-related sequence largely composed of greenschist facies volcanic and sedimentary rocks (Murphy et al., 1990). A maximum depositional age of  $613 \pm 5$  Ma (U-Pb, detrital zircon; Keppie et al., 1998) implies limited time between deposition, deformation and metamorphism of the Georgeville Group rocks and intrusion of the Greendale Complex. Intrusion of the complex is coeval with larger 615–605 Ma granitoid intrusions in the central and southern Antigonish Highlands and two smaller (and poorly exposed) appinite bodies in the southernmost highlands (Keppie et al., 1990; White et al., 2021). These relationships imply that the Greendale Complex has a similar peripheral location with respect to coeval granitoid bodies to that documented in the type area for appinites in the Scottish Caledonides. The emplacement of the Greendale Complex is interpreted to be broadly synchronous with regional strike-slip activity, which occurred after cessation of subduction (Murphy and Hynes, 1990).

The Greendale Complex consists of steeply dipping intrusive sheets ranging from ultramafic to felsic in composition thought to have been emplaced by multiple and repeated injections of compositionally diverse magma. Orientations of igneous layers within the complex are consistent with emplacement along extensional fractures during dextral shear along the Greendale and Hollow faults (Murphy and Hynes, 1990). Though the complex is largely dominated by hornblende-rich medium grained to porphyritic gabbro, abundant heterogeneity is observed at all scales with obvious mixing and mingling between units (Fig. 2a, b; Murphy et al., 1997b).

Lithologies vary in grain size from fine grained “salt and pepper” texture to pegmatite with euhedral amphibole crystals up to 15 cm in length (Fig. 2a, c, d). The pegmatitic amphiboles commonly enclose plagioclase cores and appear acicular and skeletal – these textures are attributed to rapid growth from a water-rich magma (Murphy et al., 2012). Internal contacts between intrusive units vary from sharp to gradational, planar to irregular and scalloped (Fig. 2a, b). These contacts commonly show varying degrees of assimilation and disintegration resulting in locally hybrid intermediate rocks characterized by trains of autoliths and autocrysts (Murphy et al., 1997b). Xenoliths of the host rock Morar Brook and Chisholm Brook Formation are also common, especially adjacent to external contacts.

A study of crystal-chemical parameters of white micas in Georgeville Group host rocks from the aureole of the Greendale Complex indicates emplacement at pressures of no more than 3–5 kbar (Abad et al., 2011). The Al content in hornblende (see Anderson and Smith, 1995; Putirka, 2016) supports hornblende crystallization at 5–7 kbar at temperatures between 650–750 °C (Pe-Piper and Piper, 2018).

### **3. Petrography and geochemistry**

#### **3.1 Mineralogy and textures**

The mineralogy and main textural features of the Greendale Complex are described in detail in Murphy et al. (2012) and are summarized below, further details are added where relevant. Amphibole is the overwhelmingly dominant mafic mineral in both the mafic and ultramafic rocks.

Ultramafic rocks account for 5–10 % of exposed lithologies and are dominated by hornblende, pyroxene and olivine and are classified as hornblende peridotites, pyroxene hornblendites or olivine–pyroxene hornblendites (Murphy et al., 2012; ‘corlandtites’ e.g. Bea et al., 1999). Olivine occurs as medium grained (0.1–3.5 mm) rounded hypidiomorphic chadacrysts hosted within hornblende and or clinopyroxene. The olivine ranges from Fo<sub>86</sub> to Fo<sub>75</sub>, contains inclusions of chromite and is variably altered to talc or serpentine (Fig. 3a). Pyroxene (dominantly clinopyroxene) occurs as xenomorphic to hypidiomorphic chadacrysts (0.5–6 mm) within hornblende. Clinopyroxene includes endiopside, augite and sub-calcic augite with Mg# ranging from 0.62 to 0.79. Rare orthopyroxene (hypersthene) has Mg# between 0.85 and 0.86 and very low Ca (> 0.05). Hornblende appears as two populations: 1) large (1.0–8.0 mm) hypidiomorphic oikocrysts enclosing clinopyroxene and olivine, defining a poikilitic texture (Fig. 3b, c) and 2) modally minor grains (0.5–5.0 mm), that are interstitial with plagioclase, phlogopite, and opaques. In most samples, plagioclase ranges from An<sub>50–60</sub>; rare grains with An<sub>75</sub> occur.

Mafic rocks are dominantly defined by the presence of plagioclase and hornblende. Plagioclase appears as hypidiomorphic to idiomorphic tabular grains of variable size (ca. 0.2–1.0 mm). It is typically extensively saussuritised, though euhedral forms are preserved as stubby lath-shaped crystals (Fig. 3d). Plagioclase may also have fresh irregular albitic rims that surround saussuritised cores (Fig. 3e). Interlocking grains are dominantly found in the phaneritic matrix. Plagioclase shows regular polysynthetic twinning and is typically labradorite in composition (An<sub>60–An65</sub>) with normal to oscillatory zoning also occurring (ranging from An<sub>40–An65</sub>). Hornblende occurs in mafic rocks as hypidiomorphic prismatic to acicular grains (0.5–7.0 mm)

that may contain inclusions of plagioclase and boundaries that are commonly impinged by plagioclase laths. Plagioclase inclusions contain both saussuritised cores and albitic rims which implies that this feature likely results from chemical zonation (e.g. Ca-rich core) rather than sequential growth events. Taken together, these textures indicate hornblende and plagioclase were co-precipitating liquidus phases (Fig. 3d, f).

Felsic rocks make up 5–10 % of the Greendale Complex and occur as discrete sheets, isolated pods and segregations within relatively mafic lithologies. They range from aplite to pegmatite in texture and rhyodacite to rhyolite in chemical composition. Hornblende is less abundant than in the mafic rocks and is observed as xenomorphic grains (ca. 0.5–2.0 mm) commonly pseudomorphed by chlorite and/or actinolite. Plagioclase is the dominant matrix phase and occurs as an interlocking network of heavily saussuritised tabular grains (0.5–3.0 mm). Inclusions of plagioclase within hornblende show lesser degrees of saussuritisation.

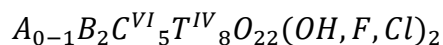
These petrographic observations suggest that two populations of hornblende occur in the suite of rocks studied. One population, dominant in ultramafic rocks, displays oikocrysts of hornblende enclosing chadacrysts of olivine and pyroxene. The other population, dominant in the mafic and felsic rocks, exhibits impinged grain boundaries and/or inclusions of plagioclase.

### **3.2 Geochemistry**

Previously published mineral geochemical data for amphiboles in mafic and ultramafic samples and lithogeochemical data for representative rock specimens (Murphy et al., 1997b; Murphy et al., 2012), are summarized here. Amphibole compositional data from felsic rocks was



not collected by previous studies. All amphiboles are calcic according to the classification of Leake et al. (2004) and their compositions are typical of igneous amphiboles. Classification is based on the following general chemical formula:



A plot of four-fold Al (Al<sup>IV</sup>, T site) vs total Al (Al<sup>tot</sup>) data from amphiboles of ultramafic and mafic rocks (Fig. 4) shows that Al resides in both Al<sup>IV</sup>, T and Al<sup>VI</sup>, C sites but appears to have a preference for the tetrahedral site, consistent with the interpretation that edenite substitution (Na,K<sup>A</sup>+Al<sup>IV</sup>=Si<sup>IV</sup>) dominates over tschermak (Al<sup>IV</sup> + Al<sup>VI</sup>= Si<sup>IV</sup> + (Fe, Mg)<sup>VI</sup> substitution (Murphy et al., 2012).

Amphiboles from ultramafic rocks are also dominated by magnesio-hornblende with low SiO<sub>2</sub> (44.3–52.1 wt.%) and Al<sub>2</sub>O<sub>3</sub> (6.2–11.9 wt.%) and high MgO (13.4–23.9 wt.%) and high Fe<sub>2</sub>O<sub>3</sub> (8.6–12.8 wt.%). A small amount of variation is observed in Mg# (0.71–0.79). Two groupings of amphiboles are distinguished on the basis of REE abundances. Group A amphiboles display a slight LREE enrichment, small negative Eu anomaly, minor decrease in HREE and significant enrichment in LILE. Group B amphiboles display enrichment in LREEs, depletion in HFSEs and HREEs and lack a negative Eu anomaly (Fig. 5). Lithogeochemical analyses of ultramafic rocks are characterized by a depletion in HFSE and high abundances of MgO (13.4–23.9 wt.%), Cr (462–2146 ppm), Ni (54–510 ppm) and Ba (< 5–246 ppm).

Amphiboles from mafic rocks are tschermakite, tschermakitic hornblende, and magnesio-hornblende in composition (Murphy et al., 2012). Amphiboles from mafic rocks have a significantly lower Mg# (0.31–0.48) than the ultramafic rocks (0.71–0.79) though amphiboles

from both rock types share a remarkably uniform Mg# over a range in Si (up to one formula unit). REE profiles are characterized by depletion in LREE ( $\text{La/Sm} \approx 0.61$ ), a slight depletion in HREE ( $\text{Gd/Yb} \approx 1.55$ ) as well as a negative Eu anomaly, which is interpreted to reflect co-precipitation of plagioclase (Group A). Compared to ultramafic rocks, lithogeochemical analyses of mafic samples have a limited range in  $\text{SiO}_2$  (45.8–52.08 wt.%), a higher  $\text{Al}_2\text{O}_3$  (17.3–19.6 wt.%), slightly lower  $\text{Fe}_2\text{O}_3$  (7.6–11.5 wt.%), and substantially lower MgO (4.0–8.6 wt.%), Ni (<5–31 ppm) and Cr (11–200 ppm). Although REE and HFSE patterns for mafic rocks have broadly similar profiles to the ultramafic rocks, depletion of HFSE (e.g. Nb, Zr and Ti) isn't as strong and they also record a pronounced negative Eu anomaly.

Intermediate to felsic rock samples have wide ranges in  $\text{SiO}_2$  (58.0–80.8 wt.%) and  $\text{Al}_2\text{O}_3$  (10.7–22.9 wt.%), but relatively low MgO (0.6–1.6 wt.%), V (6–59 ppm), and Cr (25–47 ppm). They have similar Mg# (0.33–0.48) to the mafic samples, are weakly depleted in HFSE and exhibit a pronounced negative Eu anomaly. Whole rock Sm-Nd data (Murphy and Dostal, 2007) imply an origin by crustal anatexis. Field and geochemical evidence indicate that most of the intermediate rocks formed from mixing and mingling of mafic and felsic end members (Fig. 2a).

Amphibole groups A and B (defined by contrasting REE and normalized trace element profiles) are interpreted to be coincident with the two petrographic populations outlined in the previous section (Group A = coprecipitation of hornblende and plagioclase, Group B = hornblende poikilitically enclosing olivine and clinopyroxene). As such these “geochemical groups” and “petrographic populations” will be referred to exclusively as Group A and Group B

herein. In the following discussion, groups A and B will be placed in context of their  $\delta D$  and  $\delta^{18}O$  isotopic characteristics.

#### 4. Methods

Magma systems may incorporate volatiles of several components and phases, though given the textures and amphibole rich mineralogy of the appinite suite, such features indicate that water acts as the dominant component (e.g. Murphy et al., 2012). As such, we will be focusing on the behavior of water in magmatic systems.

Individual amphibole grains were separated from hand specimens using either a Dremel microdrill or picked under binocular microscope following light crushing of specimens. Drilled samples were collected by excavating ca. 1–2 mm into fresh hornblende grains. Hand-picked grains were sonicated in distilled water to remove associated micas and powder from crushing. Fresh hornblende grains with few inclusions, and minimal or no alteration were preferentially selected to reduce contamination and the effects of late-stage alteration on analysis. For felsic samples, where late-stage alteration is widespread, grains with the least amount of alteration were selected. Petrographic observations were key in constraining the degree of alteration present in the thin sections and thus informed where rock specimens were inappropriate for sampling. Given that the methodology for isotopic analysis removes drilled or crushed/picked grains from a cut-off rather than a thin section (where textural relationships are clear), petrographic observations simply provided useful context for the degree of alteration within a given specimen number.

Oxygen was extracted from amphibole separates (ca. 0.1–0.2 mg) via silicate fluorination with excess  $\text{ClF}_3$  following the method of (Sharp, 1990). Overnight pre-fluorination at room temperature removes unbound water. Fluorination with a  $\text{CO}_2$  laser at temperatures in excess of 1500 °C results in total sample reaction and release of  $\text{O}_2$  from the mineral lattice. The  $\text{O}_2$  is converted to  $\text{CO}_2$  by reaction with hot graphite and analyzed on a VG SIRA II mass spectrometer.  $\delta^{18}\text{O}$  values reported as per mil (‰) deviations from Vienna Standard Mean Ocean Water (V-SMOW). Mineral separates for hydrogen isotopic analysis (ca. 40 mg) were degassed overnight (150 °C). Hydrogen was extracted by *in vacuo* bulk heating using the method of Donnelly et al. (2001). Water was reduced using a chromium powder furnace (830 °C) and resulting  $\text{H}_2$  (from the OH site) analyzed on a VG Optima mass spectrometer.  $\delta\text{D}$  values are reported as per mil (‰) deviations from V-SMOW. The yield (%) from hydrogen isotope analysis was used to estimate the water content (wt. %) of each sample. Water content estimates for samples should be considered as minimum estimates only as amphiboles contained variable amounts of pyroxene, olivine and feldspar inclusions in some cases. Reproducibility of O isotope data, based on repeat analyses of international and internal lab standards, was typically better than  $\pm 0.3$  ‰, with standards averaging as follows: garnet UWG-2 = 5.7 (U Wisconsin international garnet standard with accepted value = 5.8 ‰); YP-2 = 16.4 ‰ (internal quartz standard should be 16.4 ‰); SCXO = 5.2 ‰ (San Carlos olivine standard should be 5.2 ‰). Reproducibility of hydrogen isotope analyses of pure water secondary standards was better than  $\pm 2$  ‰ around the time of these analyses, with standards averaging as follows: seawater = -5 ‰ (versus accepted value of -6); Lt Std = -93 ‰ and -95 ‰ (versus accepted of -94 ‰); and GISP = -188 ‰ (versus accepted = -189 ‰).

## 5. Results

### 5.1 O and H isotopic variation

Measured  $\delta^{18}\text{O}$  and  $\delta\text{D}$  values are presented in Tables 1 and 2. The  $\delta^{18}\text{O}$  values shown in Figure 6 and Table 1, range between 0.9 ‰ and 6.8 ‰ with the lowest values recorded in the amphiboles from felsic rocks and highest values recorded in the amphiboles from ultramafic rocks. Individual ultramafic rock samples have amphibole  $\delta^{18}\text{O}$  sample averages ranging from 4.9 to 6.2 ‰ with all ultramafic samples producing a rock type average of 5.7 ‰. Amphiboles from mafic rocks have  $\delta^{18}\text{O}$  individual rock sample averages ranging from 3.6 to 5.2 ‰ with all mafic samples averaging 4.4 ‰. Amphiboles from felsic rocks have  $\delta^{18}\text{O}$  individual rock sample averages ranging from 2.1 to 3.1 ‰ with an overall rock type average of 2.6 ‰. Large variations are recorded within  $\delta\text{D}$  measured across the samples. Amphibole  $\delta\text{D}$  values range between -135 ‰ and -64 ‰ (Table 2, Fig. 7) with the highest values recorded in the amphiboles from felsic rocks (-68 to -64 ‰, average -66 ‰), moderate values in the amphiboles from mafic rocks (-106 to -88 ‰, average -99 ‰) and lowest (most D depleted) values in the amphiboles from ultramafic rocks (-135 to -88 ‰, average -103 ‰). Only sample GR5-F contained enough amphibole for H isotopic analysis from the felsic units – though there was enough to run twice. Thus, we take the value to be representative of amphiboles taken from felsic rocks as only 4 ‰ deviation is recorded between the two measurements.

### 5.2 Fractionation of fluid phase

Calculating the composition of a fluid phase that has been removed from the original mineral-fluid system requires knowledge of isotopic fractionation factors between hydrous minerals and fluid. Fractionation factors are influenced by temperature, pressure, fluid

composition and mineral composition (Chacko et al., 2001). Most fractionation factors are derived from experimentally determined mineral-mineral fractionations as summarized in Chacko et al. (2001) and Valley (2003). However, as no experimental data are available for O isotopic fractionation in amphiboles, estimates of fractionation are based on theoretical predictions (Zheng, 1993). Although this practice is inferior to experimentally derived fractionation, until further studies have been completed, we are implementing the best available values. Difficulty arises with amphibole-water H isotope fractionations given by Suzuoki and Epstein (1976) and Graham et al. (1984), which show differences related to the effects of Fe on mineral-water fractionations. Some of the differences are likely due to differences in pressures used during their experiments, however the reason for this is not fully understood (Chacko et al., 2001; Marks et al., 2004). No clear inverse relationship is visible between measured  $\delta D$  and  $Fe_{(tot)}$  as would be expected by Suzuoki and Epstein (1976; Fig. 8a), though given potential errors involved in estimations of  $Fe^{3+}/Fe^{2+}$  ratios from electron microprobe analysis (e.g. Feldstein et al., 1997) we do not take this to favour one set of calculations over the other.

The measured  $\delta^{18}O$  and  $\delta D$  of the amphiboles can be used to calculate the isotopic composition of the fluid phase the amphiboles precipitate from. Amphibole-water oxygen isotope fractionation at a temperature average of 700 °C is -2.3 ‰ (expressed as  $1000\ln\alpha_{amph-water}$ ) according to the equations of Zheng (1993). This produces a  $\delta^{18}O$  fluid isotopic composition of 3.1 to 9.1 ‰ (see Table 1). Amphibole-water hydrogen isotope fractionations at 700 °C can be as large as -32 ‰ (Graham et al., 1984) or as low as -17 ‰ (Suzuoki and Epstein, 1976). This produces a fluid phase composition of -118 to -47 ‰ for the calculations of Graham et al. (1984) and -103 to -32 ‰ for the calculations of Suzuoki and

Epstein (1976; see Table 2). Calculated fluid  $\delta^{18}\text{O}$  and  $\delta\text{D}$  are plotted against each other in Figure 9a, b.

## **6. Discussion**

### **6.1 Pressure-Temperature constraints**

The calculation of pressure-temperature (P-T) conditions in igneous rocks may be used to estimate the depth of magma crystallization and/or emplacement. When compared to mineral and fluid isotope signatures, these two data sources may be used to derive if a given mineral precipitated at the fluid source or away from it (e.g. Ulrych et al., 2018). The Greendale Complex is interpreted to have been emplaced at shallow structural levels during dextral motion along strike-slip faults (Murphy and Hynes, 1990). The abundance of pegmatitic hornblende gabbro, widespread roof pendants, and miarolitic cavity textures indicate the Greendale Complex is exposed near the pluton roof (Murphy et al., 2012).

Both Group A and Group B amphiboles are igneous in composition and their geochemistry is sensitive to changes in pressure and temperature as well as magma composition. A variety of amphibole-based thermobarometers have been proposed to estimate P-T conditions of crystallization for different igneous systems (e.g. Putirka, 2016; Ridolfi and Renzulli, 2012). Although the thermobarometer of Ridolfi and Renzulli (2012) is suitable for the host rock composition, we deem it unsuitable for the purposes of this study as its sensitivity to compositional variations in amphibole may introduce large uncertainties in estimations of crystallization conditions (Ulrych et al., 2018). Although the Al content of hornblende indicates crystallization at 5–7 kbar and between 650–750 °C (Anderson and Smith, 1995; Pe-Piper and

Piper, 2018), Figure 10a suggests that temperature conditions could have been closer to 650 °C which supports crystallization between 5–8 kbar. The empirical barometer of Pál-Molnár et al. (2015), calibrated using the Al<sub>2</sub>O<sub>3</sub> contents of experimentally produced amphiboles, suggests crystallization pressures concentrated between 6.7–9.0 kbar, though significant variation of pressure is observed across Al<sub>2</sub>O<sub>3</sub> contents. Results using calculations in Pe-Piper and Piper (2018) are thus preferred. Comparing the Al<sub>2</sub>O<sub>3</sub> contents of Greendale Complex amphiboles against the calculations of Anderson and Smith (1995) shows crystallization predominantly occurred between 7–8 kbar at or near to 650 °C (Fig. 10b). Given the emplacement depth is likely between 3–5 kbar (Abad et al., 2011), it appears that a significant proportion of hornblende growth occurred at deeper structural levels, but was transported upwards by ascending magma.

## 6.2 Oxygen isotopes

Oxygen is the most abundant element in ordinary rocks, making up approximately 50 wt. %, thus silicate oxygen has a major influence on the observed  $\delta^{18}\text{O}$  for the water-to-rock ratios that likely exist in these systems. The  $\delta^{18}\text{O}$  of a mineral and the related fluid from which it crystallizes or re-equilibrates with, may be determined by the exchange of oxygen between the mineral and fluid, and the temperature at which this exchange occurs (Sheppard, 1986a). Equilibrium  $\delta^{18}\text{O}$  values of igneous minerals decrease as follows: quartz > alkali-feldspar > calcic plagioclase > biotite > apatite > orthopyroxene > zircon > clinopyroxene > amphibole > garnet > olivine > oxides (Eiler, 2001; Valley, 2003). Minerals such as olivine, magnetite and amphibole typically have lower  $\delta^{18}\text{O}$  values than basaltic melts at magmatic temperatures and so precipitation of these minerals increases  $\delta^{18}\text{O}$  in the residual melt. However, crystallization and fractionation of quartz or albitic plagioclase or K-feldspar from a melt deplete the residual melt



in  $^{18}\text{O}$  (Bucholz et al., 2017). Relicts of clinopyroxene and olivine, which are the most significant inclusions in amphibole samples, have a limited effect on the range in  $\delta^{18}\text{O}$  values because pyroxene and olivine fractionation have a similar effect to amphibole (Zheng, 1993). Study of variations in oxygen isotopic composition in magmas during fractional crystallization indicate that higher temperature systems should experience limited increases in  $\delta^{18}\text{O}$  (Taylor, 1968).

The sampling method for isotopic analysis removes grains from their textural relationships, therefore it is not possible to directly correlate isotopic results with groups A and B as defined by their REE profiles, trace element abundances and petrographic observations. However, there are two distinct isotopic signatures (e.g. Fig. 6), which trace the origin and depth of fluids from which the two amphibole populations precipitate. We interpret these two distinct isotopic signatures to likely represent the same processes acting to form the two petrographic and geochemical populations previously described.

*Group B amphibole:* In general, minerals crystallizing in equilibrium with mantle-derived magmas and fluids typically exhibit a restricted O isotopic range of  $5.3 \pm 0.6$  ‰ (Valley et al., 1998) or 5.3–5.6 ‰ (amphibole, Chazot et al., 1997) or  $5.5 \pm 0.2$  ‰ (MORB, Bindeman, 2008). The first two studies imply that Group B amphiboles in both ultramafic samples (4.0–6.8 ‰) and mafic samples (2.5–5.3 ‰) have predominantly mantle-derived water (which is supported by petrographic observations where mafic and ultramafic samples both contain Group B amphiboles). Whereas the final study implies only ultramafic Group B amphiboles contain mantle-derived water (Fig. 6). Geochemical analyses show depletion of ultramafic rocks in HFSE and high abundances of MgO, Cr, Ni and Ba. These geochemical signatures support a

mantle fluid source in a subduction zone setting (Atherton and Ghani, 2002; Pearce, 1983). Elevated O isotopic values ( $> 5.9\text{‰}$ ), as seen in Figure 6, are typically attributed to low T melting or assimilation of supracrustal sedimentary or volcanic rocks (Valley et al., 2005).

The range in Group B amphibole values (ca.  $4.7\text{--}6.8\text{‰}$ ) suggests that the water was largely mantle-derived. Given that the amphiboles likely crystallized at depths equivalent to 5–8 kbar, these data imply that this water was dissolved in mantle-derived magma and ascended to a depth of ca. 12–16 km whereupon Group B amphiboles began to crystallize. This scenario is broadly consistent with that depicted by Collins et al. (2020) in which subduction generates hydrous basaltic magmas in the overlying mantle wedge that exsolve water as they cool beneath the Moho.

Some amphiboles retained mantle-like  $\delta^{18}\text{O}$  values, whereas others with high  $\delta^{18}\text{O}$  may have partially re-equilibrated during low T water-rock interactions in supracrustal conditions. This is similar to the manner described by Pitcher (1997), olivine-pyroxene-hornblende textural relationships in appinites are interpreted to result from the upward transport and hydration of olivine-pyroxene cumulates in water-rich mafic magma. These cumulates reacted to form amphibole during ascent. Group B amphiboles in mafic and ultramafic rocks display a poikiloblastic texture of oikocrysts of hornblende enclosing chadacrysts of olivine and pyroxene. Textural relations support the sequence of timing suggested by Pitcher (1997), however, olivine and pyroxene did not react to form hornblende (Fig. 3b, c).

401 *Group A amphibole:* The lower  $\delta^{18}\text{O}$  values ( $< 4.7\text{ ‰}$ ) of Group A amphiboles indicate their  
402 fluid source was contaminated by high-T hydrothermal cycling of meteoric water into shallow  
403 (epizonal) magma systems before or during crystallization (Bindeman, 2008). Petrographic  
404 observations show extensive saussuritisation of plagioclase and pseudomorphing of hornblende  
405 by chlorite and/or actinolite, supporting availability of excess fluids during and/or after  
406 crystallization. Field evidence for extensive mixing and mingling between intrusive phases  
407 (Murphy et al., 1997b) suggests that the water source for some Group A amphiboles may have  
408 come from earlier hydrothermally altered appinite sheets (see Valley, 2003; Valley et al., 2005).  
409 According to Boroughs et al. (2012), direct interaction of crystallizing magma and meteoric  
410 water is improbable because 1) meteoric-hydrothermal systems commonly reside at significantly  
411 lower pressures than magmatic systems, and 2) magmas cannot ingest enough fluid to produce  
412 very low  $\delta^{18}\text{O}$  magma. Studies have shown that assimilated hydrothermally altered country rock  
413 can produce relatively small shifts ( $< 2\text{ ‰}$ ) in  $\delta^{18}\text{O}$  (Wolff et al., 2002). Thus, water  
414 accompanying crystallization of Group A amphiboles was possibly sourced from previously  
415 intruded hydrothermally altered sheets.

416  
417 Oxygen isotope exchange between hornblende and feldspar at decreasing temperatures  
418 may also result in a negative  $\delta^{18}\text{O}$  shift (Demény et al., 2008). Hornblende oxygen-self-diffusion  
419 closure temperatures are around 600–800 °C (at 100–1000 °C  $\text{Ma}^{-1}$  cooling rate and 0.1–1.0 mm  
420 grain size; Farver, 1989). These temperatures are broadly compatible with crystallization  
421 temperatures for hornblende of the Greendale Complex (650–750 °C; Pe-Piper & Piper, 2018),  
422 implying that oxygen isotope exchange between hornblende and feldspar was only possible

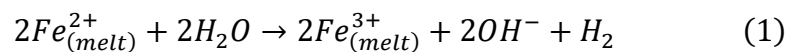
during crystallization of the hornblende, therefore unlikely to solely responsible for the negative  $\delta^{18}\text{O}$  shift.

The calculated composition of the fluid  $\delta^{18}\text{O}$  from which the amphiboles crystallized ranges from 3.1 to 9.1 ‰. The spread of these values support heterogeneity in the amphibole water source.

### 6.3 Hydrogen isotopes

Hydrogen is usually a trace element in rocks (ca. < 2000 ppm), a rock with 1 wt. %  $\text{H}_2\text{O}$  contains approximately 0.11 wt % hydrogen. In contrast to oxygen (ca. 50 wt. %), this means the hydrogen budget is more strongly influenced by the interacting fluid (Sheppard, 1986a). Due to limited fractionation of  $\delta\text{D}$  between amphiboles and mantle fluids ( $-80 \pm 5$  ‰ from pristine MORB glasses, Kyser and O'Neil, 1984),  $\delta\text{D}$  variations in amphiboles and associated fluids from which they crystallize may be interpreted to reflect mantle heterogeneities and/or the influence of crustal contamination and metasomatic fluids within mantle-derived rocks. Amphiboles analyzed in this study have highly D-depleted isotopic compositions ( $\delta\text{D} = -135$  ‰ to  $-64$  ‰) when compared to the normal range for mantle amphiboles (ca.  $\delta\text{D} = -100$  to  $-20$  ‰; Hoefs, 2018 and references therein). Various explanations have been proposed to explain low  $\delta\text{D}$  amphibole values in magmatic rocks:

1. *Oxidation of  $\text{Fe}^{2+}$  to  $\text{Fe}^{3+}$  in magmas.* This causes degassing of molecular  $\text{H}_2$  (Mathez, 1984; Sato, 1978), which can result in enrichment in D in the residual phases (e.g. Kyser 1986) via reaction (1).



Released molecular hydrogen is typically depleted in deuterium relative to water. Thus, if amphibole crystallizes at increasingly oxidizing conditions with significant degassing, there should be a resulting increase in the  $\delta D$  of amphibole with increasing  $Fe^{3+}/Fe^{2+}$  ratios (Kyser, 1986; Marks et al., 2004). However, the variations in  $\delta D$  show a weak inverse correlation with  $Fe^{3+}/Fe^{2+}$  (Fig. 8b), suggesting that variations in oxidation state of the magma cannot account for the low values or the range in amphibole  $\delta D$ .

2. *Major degassing of magmatic water.* Experimental studies by Kuroda et al. (1982) and Dobson et al. (1989) show that water exsolved from a melt may be enriched (+20 to +50 ‰) in  $\delta D$  relative to the remaining melt. Exsolved water ascends and percolates to upper parts of the magma system (Agemar et al., 1999; Collins et al., 2020). According to Rayleigh-type models, degassing should be characterized by a correlation of exponentially decreasing  $\delta D$  values and decreasing water content in magmatic rocks or constituent minerals (Marks et al., 2004; Taylor et al., 1983). In our data set however, on average, the lowest  $\delta D$  values are more typically derived from the less fractionated ultramafic-mafic samples that dominantly contain Group B amphibole, which are less evolved than Group A amphibole (Murphy et al., 2012), which is inconsistent with the degassing trend (Fig. 11a, b). Furthermore, the extreme water loss required to acquire the low  $\delta D$  values would destabilize formation of late amphibole (Marks et al., 2004). Magmatic degassing is thus not regarded as a viable process to explain the low  $\delta D$  values.

3. *Input of volatiles from recycled oceanic lithosphere.* Mixing between a water-rich high  $\delta D$  subduction-related component and a separate component characterized by water-poor and low  $\delta D$  has been proposed as a possible explanation for linear trends between  $H_2O$

(wt. %) and  $\delta D$  (Shaw et al., 2008, 2012). Experimentally determined fractionation factors between hydrous minerals and water indicate that fluid released from a dehydrating subducting slab, should be D-enriched (Graham et al., 1984; Suzuoki and Epstein, 1976; Vennemann and O'Neil, 1996). Consequently, recycled oceanic lithosphere is predicted to yield a low  $\delta D$  water component as the progressively dehydrated slab releases D-enriched fluids into the overlying mantle wedge (Shaw et al., 2008). Given the field evidence for extensive mingling between intrusive phases (Murphy et al., 1997b), this process is unlikely to be solely responsible for the  $\delta D$  isotopic signature, however it explains the linear trend of amphibole  $\delta D$  values with water content and is thus interpreted to be a dominant source of fluids for ultramafic-mafic samples of Group B amphiboles (ca.  $< -100$  ‰; outside the normal mantle amphibole range provided in Hoefs, 2018 and references therein).

4. *Influx of hydrothermal-meteoric fluids during crystallization* (e.g. Agemar et al., 1999).

This process is consistent with the abundance of low  $\delta^{18}O$  values ( $< 4.7$  ‰) found dominantly within mafic and felsic amphiboles (Group A), which support a fluid source from previously intruded hydrothermally altered sheets. This process could thus explain some of the  $\delta D$  signatures found within some felsic and mafic rocks ( $\delta D$  -106 to -64 ‰). However, it does not explain the anomalously low  $\delta D$  values abundant in the ultramafic rocks, which dominantly contain Group B amphiboles from petrographic observations and have mantle-like  $\delta^{18}O$  values.

5. *Fluid input derived from organic matter and/or assimilation of organic-rich sedimentary rocks* (e.g. Sheppard, 1986b). The Hollow Fault (Fig. 1c) was active during magma emplacement and directed fluid and magma migration, mixing and mingling from various

sources and crustal levels (Murphy and Hynes, 1990). Assimilation of organic-rich sediments such as those of the Morar Brook Formation or fluid derived from such sediments can explain why a portion of  $\delta D$  and  $\delta^{18}O$  fluid values do not plot in the magmatic  $H_2O$  field, and instead lie within the organic waters field ( $\delta D$  ca.  $< -90$  ‰; Fig. 9a, b). This process is consistent with high  $\delta^{18}O$  values ( $> 5.9$  ‰) related to low T supracrustal contamination for Group B amphiboles (Valley et al., 2005).

Amphibole-water  $\delta D$  isotope fractionations at 700 °C can be as large as -32 ‰ (Graham et al., 1984) or as low as -17 ‰ (Suzuoki and Epstein, 1976). However, the range in values is much smaller than the observed variations in  $\delta D$  and given the poor correlation to amphibole Fe-content, neither can explain the range of values measured. Thus, the data supports heterogeneity in the  $\delta D$  isotopic composition of the source fluid rather than fractionation from it.

#### **6.4 Summary and implications**

Appinites may, in principle, form in any tectonic environment in which mafic magmas become anomalously water-rich. However, geochemical, geochronological and field studies indicate appinite complexes are preferentially emplaced after the cessation of subduction (Atherton and Ghani, 2002; Murphy, 2013, 2020 and references therein). In the aftermath of continent-continent collision, such as in the Variscan belt of continental Europe, appinitic magma may be generated by decompression melting (e.g. Castro et al., 2003). The Greendale Complex, however, is one of several late Neoproterozoic appinite complexes documented in Avalonia and Cadomia, two neighboring terranes located along the northern Gondwanan margin at that time. Regional syntheses indicate that in each region, these complexes were emplaced at

the termination of arc magmatism, which is interpreted to reflect ridge-trench collision and the diachronous propagation of a San Andreas-style transform fault along the length of the northern Gondwanan margin (Murphy and Nance, 1989). Such an environment generates a slab window setting on the landward side of the transform fault that enables asthenospheric upwelling and the generation of mafic magmas (Fig. 12; e.g. Johnston and Thorkelson, 1997; Sisson et al., 2003).

Upwelling asthenosphere advects heat into an overlying continental lithospheric mantle previously metasomatised by subduction-derived fluids and underplating hydrous mafic magmas. Experimental evidence indicating that much of this water is stored in calcic amphiboles (such as pargasite) is supported by the widespread occurrence of pargasite in xenoliths from several supra-subduction zone localities (Corgne et al., 2018 and references therein). In the case of the Greendale Complex, asthenospheric upwelling induced melting of a previously hydrated continental lithospheric mantle. This scenario is consistent with Sm-Nd isotopic values of mafic rocks in the Greendale Complex, which are significantly lower than the contemporary depleted mantle and lie within the Avalonian envelope for the Neoproterozoic-Paleozoic evolution of its lithospheric mantle (Murphy et al., 1997b; Murphy and Dostal, 2007). Melting of this hydrated mantle formed a fluid-rich mafic (appinitic) magma. The high  $\delta^{18}\text{O}$  values of Group B amphiboles (between 4.7–5.9 ‰) reflect incorporation of mantle-derived fluids into the crystal structure. These mantle-derived fluids were initially extracted from the vicinity of a dehydrated (D-depleted) subducting slab producing anomalously low  $\delta\text{D}$  values (ca.  $< -100$  ‰) and contaminated the overlying lithospheric mantle wedge either directly (as fluids) or indirectly as hydrous magma which exsolved water as it cooled beneath the Moho (e.g. Collins et al., 2020). This water then became incorporated into appinitic magmas when heat was advected into the



continental lithospheric mantle by asthenospheric upwelling, resulting in progressively D-enriched signatures as supported by the linear trend between  $\delta D$  and water contents (wt. %). Hornblende compositions (Murphy et al., 2012; Pe-Piper and Piper, 2018) indicate equilibration between 3–7 kbar suggesting that mantle water dissolved in the magma and became incorporated into the hornblende structure as the magma rose through the crust by exploiting the Hollow-Greendale fault system. Textures indicative of high growth rate (Murphy and Hynes, 1990) are consistent with rapid ascent of magma as it exploited this fault system.

As the magma migrated further upwards in the crust, it was contaminated by assimilation of organic-rich host rock (which provided a fluid source for supracrustal Group B amphiboles,  $\delta^{18}O > 5.9$  ‰, some  $\delta D$  signatures  $< -90$  ‰) and/or by previously hydrothermally altered bodies (dominant fluid source for Group A amphiboles,  $\delta^{18}O < 4.7$  ‰,  $\delta D$  ca.  $-106$  to  $-64$  ‰). Overlap between isotopic signatures emphasizes that these processes are not mutually exclusive and that fluid interaction in subduction zones represents a dynamic system. The Hollow-Greendale fault system likely facilitated assimilation into the magma of 1) fluids derived from previously hydrothermally altered bodies, and 2) supracrustal rocks and associated fluids from organic sediments at low T. Felsic  $\delta D$  values are significantly higher and show extensive  $\delta^{18}O$  variation when compared to amphibole isotopic signatures from mafic and ultramafic rocks. The late-stage intrusion history of felsic magmas and their extensive alteration implies they likely formed separately to the ultramafic and mafic magmas. This interpretation is compatible with field evidence of extensive mingling between intrusive phases (Murphy et al., 1997b).

## Acknowledgments

This project was initiated when IPC was in receipt of a Laidlaw scholarship at the University of St Andrews and was made possible by grant funding from the Geological Society of London (Joseph Burr Tyrrell Fund) and by NSERC, Canada (2020-03872). The authors are thankful to the analytical scientists at SUERC, UK for their time and patience spent aiding in collection of the isotopic data. Constructive and insightful comments from Mike Fowler and Antonio Castro greatly improved this manuscript.

## References

- Abad, I., Murphy, J.B., Nieto, F., Gutiérrez-Alonso, G., Walsh, E., 2011. Distinction Between Deformation and Contact Metamorphism by Very Low-Grade Metamorphism Indicators in the Georgeville Group (Nova Scotia, Canada), in: The Interrelationship Between Deformation and Metamorphism, University of Granada. pp. 38–39.
- Agemar, T., Wörner, G., Heumann, A., 1999. Stable isotopes and amphibole chemistry on hydrothermally altered granitoids in the North Chilean Precordillera: A limited role for meteoric water? *Contributions to Mineralogy and Petrology* 136, 331–344.  
<https://doi.org/10.1007/s004100050542>
- Anderson, J.L., Smith, D.R., 1995. The effects of temperature and fO<sub>2</sub> on the Al-in-hornblende barometer. *American Mineralogist* 80, 549–559. <https://doi.org/10.2138/am-1995-5-614>
- Atherton, M.P., Ghani, A.A., 2002. Slab breakoff: A model for Caledonian, Late Granite syn-collisional magmatism in the orthotectonic (metamorphic) zone of Scotland and Donegal, Ireland. *Lithos* 62, 65–85. [https://doi.org/10.1016/S0024-4937\(02\)00111-1](https://doi.org/10.1016/S0024-4937(02)00111-1)
- Bea, F., Montero, P., Molina, J.F., 1999. Mafic Precursors, Peraluminous Granitoids, and Late Lamprophyres in the Avila Batholith: A Model for the Generation of Variscan Batholiths in

583 Iberia. *The Journal of Geology* 107, 399–419. <https://doi.org/10.1086/314356>

584 Bindeman, I., 2008. Oxygen Isotopes in Mantle and Crustal Magmas as Revealed by Single  
585 Crystal Analysis. *Reviews in Mineralogy and Geochemistry* 69, 445–478.  
586 <https://doi.org/10.2138/rmg.2008.69.12>

587 Borouhgs, S., Wolff, J.A., Ellis, B.S., Bonnichsen, B., Larson, P.B., 2012. Evaluation of models  
588 for the origin of Miocene low- $\delta^{18}\text{O}$  rhyolites of the Yellowstone/Columbia River Large  
589 Igneous Province. *Earth and Planetary Science Letters* 313–314, 45–55.  
590 <https://doi.org/10.1016/j.epsl.2011.10.039>

591 Bowes, D.R., McArthur, A.C., 1976. Nature and Genesis of the Appinite Suite. *Krystalinikum*  
592 12, 31–46.

593 Bucholz, C.E., Jagoutz, O., Vantongeren, J.A., Setera, J., Wang, Z., 2017. Oxygen isotope  
594 trajectories of crystallizing melts: Insights from modeling and the plutonic record.  
595 *Geochimica et Cosmochimica Acta* 207, 154–184.  
596 <https://doi.org/10.1016/j.gca.2017.03.027>

597 Castro, A., Corretgé, L.G., Rosa, J.D.D.L.R., Fernández, C., López, S., García-Moreno, O.,  
598 Chacón, H., 2003. The Appinite-Migmatite Complex of Sanabria, NW Iberian Massif,  
599 Spain. *Journal of Petrology* 44, 1309–1344. <https://doi.org/10.1093/petrology/44.7.1309>

600 Chacko, T., Cole, D.R., Horita, J., 2001. Equilibrium Oxygen, Hydrogen and Carbon Isotope  
601 Fractionation Factors Applicable to Geologic Systems. *Reviews in Mineralogy and*  
602 *Geochemistry* 43, 1–81. <https://doi.org/10.2138/gsrmg.43.1.1>

603 Chazot, G., Lowry, D., Menzies, M., Matthey, D., 1997. Oxygen isotopic composition of hydrous  
604 and anhydrous mantle peridotites. *Geochimica et Cosmochimica Acta* 61, 161–169.  
605 [https://doi.org/10.1016/S0016-7037\(96\)00314-6](https://doi.org/10.1016/S0016-7037(96)00314-6)

606 Collins, W.J., Murphy, J.B., Johnson, T.E., Huang, H.Q., 2020. Critical role of water in the  
 607 formation of continental crust. *Nature Geoscience* 13, 331–338.  
 608 <https://doi.org/10.1038/s41561-020-0573-6>

609 Corgne, A., Schilling, M.E., Grégoire, M., Langlade, J., 2018. Experimental constraints on  
 610 metasomatism of mantle wedge peridotites by hybridized adakitic melts. *Lithos* 308–309,  
 611 213–226. <https://doi.org/10.1016/j.lithos.2018.03.006>

612 Demény, A., Casillas, R., Vennemann, T.W., Hegner, E., Nagy, G., Ahijado, A., De La Nuez, J.,  
 613 Sipos, P., Pilet, S., Milton, J., 2008. Plume-related stable isotope compositions and fluid–  
 614 rock interaction processes in the Basal Complex of La Palma, Canary Islands, Spain, in:  
 615 Coltorti, M., Grégoire, M. (eds.), *Metasomatism in Oceanic and Continental Lithospheric*  
 616 *Mantle*. Geological Society, London, Special Publications, pp. 155–175.  
 617 <https://doi.org/10.1144/SP293.8>

618 Dobson, P.F., Epstein, S., Stolper, E.M., 1989. Hydrogen isotope fractionation between  
 619 coexisting vapor and silicate glasses and melts at low pressure. *Geochimica et*  
 620 *Cosmochimica Acta* 53, 2723–2730. [https://doi.org/10.1016/0016-7037\(89\)90143-9](https://doi.org/10.1016/0016-7037(89)90143-9)

621 Donnelly, T., Waldron, S., Tait, A., Dougans, J., Bearhop, S., 2001. Hydrogen isotope analysis  
 622 of natural abundance and deuterium-enriched waters by reduction over chromium on-line to  
 623 a dynamic dual inlet isotope-ratio mass. *Rapid communications in mass spectrometry* 15,  
 624 1297–1303. <https://doi.org/10.1002/rcm.361>

625 Eiler, J.M., 2001. Oxygen Isotope Variations of Basaltic Lavas and Upper Mantle Rocks.  
 626 *Reviews in Mineralogy and Geochemistry* 43, 319–364.  
 627 <https://doi.org/10.2138/gsrmg.43.1.319>

628 Farver, J.R., 1989. Oxygen self-diffusion in diopside with application to cooling rate

629 determinations. *Earth and Planetary Science Letters* 92, 386–396.  
 630 [https://doi.org/10.1016/0012-821X\(89\)90062-9](https://doi.org/10.1016/0012-821X(89)90062-9)  
 631 Feldstein, S.N., Lange, R.A., Vennemann, T., O’Neil, J.R., 1997. Ferric-ferrous ratios, H<sub>2</sub>O  
 632 contents and D/H ratios of phlogopite and biotite from lavas of different tectonic regimes.  
 633 *Contributions to Mineralogy and Petrology* 126, 51–66.  
 634 <https://doi.org/10.1007/s004100050235>  
 635 Fowler, M.B., 1988. Elemental evidence for crustal contamination of mantle-derived Caledonian  
 636 syenite by metasediment anatexis and magma mixing. *Chemical Geology* 69, 1–16.  
 637 [https://doi.org/10.1016/0009-2541\(88\)90154-4](https://doi.org/10.1016/0009-2541(88)90154-4)  
 638 Fowler, M., Rollinson, H., 2012. Phanerozoic sanukitoids from Caledonian Scotland:  
 639 Implications for Archean subduction. *Geology* 40, 1079–1082.  
 640 <https://doi.org/10.1130/G33371.1>  
 641 Fowler, M.B., Henney, P.J., Darbyshire, D.P.F., Greenwood, P.B., 2001. Petrogenesis of high  
 642 Ba–Sr granites: the Rogart pluton, Sutherland. *Journal of the Geological Society* 158, 521–  
 643 534. <https://doi.org/10.1144/jgs.158.3.521>  
 644 Graham, C.M., Harmon, R.S., Sheppard, S.M.F., 1984. Experimental hydrogen isotope studies:  
 645 hydrogen isotope exchange between amphibole and water. *American Mineralogist* 69, 128–  
 646 138.  
 647 Hibbard, J.P., Staal, C.R. V, Rankin, D.W., 2007. A comparative analysis of pre-Silurian crustal  
 648 building blocks of the northern and the southern Appalachian orogen. *American Journal*  
 649 *of Science* 307, 23–45. <https://doi.org/10.2475/01.2007.02>  
 650 Hoefs, J., 2018. *Stable Isotope Geochemistry*, 8th ed. Springer International Publishing AG.  
 651 Johnston, S.T., Thorkelson, D.J., 1997. Cocos–Nazca slab window beneath Central America.

652 Earth and Planetary Science Letters 146, 465–474. <https://doi.org/10.1016/S0012->  
 653 821X(96)00242-7

654 Keppie, J.D., Dallmeyer, R.D., Murphy, J.B., 1990. Tectonic implications of  $^{40}\text{Ar}/^{39}\text{Ar}$   
 655 hornblende ages from late Proterozoic-Cambrian plutons in the Avalon Composite Terrane,  
 656 Nova Scotia, Canada. Geological Society of America Bulletin 102, 516–528.  
 657 [https://doi.org/10.1130/0016-7606\(1990\)102%3C0516:TIOAAH%3E2.3.CO;2](https://doi.org/10.1130/0016-7606(1990)102%3C0516:TIOAAH%3E2.3.CO;2)

658 Keppie, J.D., Davis, D.W., Krogh, T.E., 1998. U-Pb geochronological constraints on  
 659 Precambrian stratified units in the Avalon Composite Terrane of Nova Scotia, Canada:  
 660 tectonic implications. Canadian Journal of Earth Sciences 35, 222–236.  
 661 <https://doi.org/10.1139/e97-109>

662 Keppie, J.D., Dostal, J., Murphy, J.B., Nance, R.D., 1996. Terrane transfer between eastern  
 663 Laurentia and western Gondwana in the early Paleozoic: Constraints on global  
 664 reconstructions, in: Nance, R.D., Thompson, M.D. (eds.), Avalonian and Related Peri-  
 665 Gondwanan Terranes of the Circum North Atlantic. Geological Society of America Special  
 666 Paper 304, pp. 369–380. <https://doi.org/10.1130/0-8137-2304-3.369>

667 Kuroda, Y., Hariya, Y., Suzuoki, T., Matsuo, S., 1982. D/H fractionation between water and the  
 668 melts of quartz, K-feldspar, albite and anorthite at high temperature and pressure.  
 669 Geochemical Journal 16, 73–78. <https://doi.org/10.2343/geochemj.16.73>

670 Kyser, T.K., 1986. Stable isotope variations in the mantle, in: Valley, J.W., Taylor, H.P., O’Neil,  
 671 J.R. (eds.), Stable Isotopes. Reviews in Mineralogy and Geochemistry, pp. 141–162.

672 Kyser, T.K., O’Neil, J.R., 1984. Hydrogen isotope systematics of submarine basalts. Geochimica  
 673 et Cosmochimica Acta 48, 2123–2133. [https://doi.org/10.1016/0016-7037\(84\)90392-2](https://doi.org/10.1016/0016-7037(84)90392-2)

674 Leake, B.E., Woolley, A.R., Birch, W.D., Burke, E.A.J., Ferraris, G., Grice, J.D., Hawthorne,

675 F.C., Kisch, H.J., Krivovichev, V.G., Schumacher, J.C., Stephenson, N.C.N., Whittaker,  
 676 E.J.W., 2004. Nomenclature of amphiboles: Additions and revisions to the International  
 677 Mineralogical Association's amphibole nomenclature. *American Mineralogist* 89, 883–887.  
 678 <https://doi.org/10.1180/0026461046810182>

679 Marks, M., Vennemann, T., Siebel, W., Markl, G., 2004. Nd-, O-, and H-isotopic evidence for  
 680 complex, closed-system fluid evolution of the peralkaline Ilímaussaq intrusion, south  
 681 Greenland. *Geochimica et Cosmochimica Acta* 68, 3379–3395.  
 682 <https://doi.org/10.1016/j.gca.2003.12.008>

683 Mathez, E.A., 1984. Influence of degassing on oxidation states of basaltic magmas. *Nature* 310,  
 684 371–375. <https://doi.org/10.1038/310371a0>

685 Moore, G., Carmichael, I.S.E., 1998. The hydrous phase equilibria (to 3 kbar) of an andesite and  
 686 basaltic andesite from western Mexico: constraints on water content and conditions of  
 687 phenocryst growth. *Contributions to Mineralogy and Petrology* 130, 304–319.  
 688 <https://doi.org/10.1007/s004100050367>

689 Müntener, O., Kelemen, P.B., Grove, T.L., 2001. The role of H<sub>2</sub>O during crystallization of  
 690 primitive arc magmas under uppermost mantle conditions and genesis of igneous  
 691 pyroxenites: an experimental study. *Contributions to Mineralogy and Petrology* 141, 643–  
 692 658. <https://doi.org/10.1007/s004100100266>

693 Murphy, J.B., 2013. Appinite suites: A record of the role of water in the genesis, Transport,  
 694 Emplacement and crystallization of magma. *Earth-Science Reviews* 119, 35–59.  
 695 <https://doi.org/10.1016/j.earscirev.2013.02.002>

696 Murphy, J.B., 2020. Appinite suites and their genetic relationship with coeval voluminous  
 697 granitoid batholiths. *International Geology Review* 62, 1–31.

698       <https://doi.org/10.1080/00206814.2019.1630859>

699   Murphy, J.B., Dostal, J., 2007. Continental mafic magmatism of different ages in the same  
700       terrane: Constraints on the evolution of an enriched mantle source. *Geology* 35, 335–338.  
701       <https://doi.org/10.1130/G23072A.1>

702   Murphy, J.B., Hynes, A.J., 1990. Tectonic control on the origin and orientation of igneous  
703       layering: An example from the Greendale Complex, Antigonish Highlands, Nova Scotia,  
704       Canada. *Geology* 18, 403–406. [https://doi.org/10.1130/0091-](https://doi.org/10.1130/0091-7613(1990)018<0403:TCOTOA>2.3.CO;2)  
705       7613(1990)018<0403:TCOTOA>2.3.CO;2

706   Murphy, J.B., Blais, S.A., Tubrett, M., McNeil, D., Middleton, M., 2012. Microchemistry of  
707       amphiboles near the roof of a mafic magma chamber: Insights into high level melt  
708       evolution. *Lithos* 148, 162–175. <https://doi.org/10.1016/j.lithos.2012.06.012>

709   Murphy, J.B., Keppie, J.D., Davis, D., Krogh, T.E., 1997a. Regional significance of new U-Pb  
710       age data for Neoproterozoic igneous units in Avalonian rocks of northern mainland Nova  
711       Scotia, Canada. *Geological Magazine* 134, 113–120.  
712       <https://doi.org/10.1017/S0016756897006596>

713   Murphy, J.B., Hynes, A.J., Cousens, B., 1997b. Tectonic influence on Late Proterozoic  
714       Avalonian magmatism: An example from the Greendale complex, Antigonish Highlands,  
715       Nova Scotia, Canada, in: Sinha, A.K., Whalen, J.B., Hogan, J.P. (eds.), *Geological Survey*  
716       *of America Memoir* 191. pp. 255–274. <https://doi.org/10.1130/0-8137-1191-6.255>

717   Murphy, J.B., Keppie, J.D., Dostal, J., Hynes, A.J., 1990. Late Precambrian Georgeville group: a  
718       volcanic arc rift succession in the Avalon Terrane of Nova Scotia. *Geological Society*  
719       *London, Special Publication* 51, 383–393. <https://doi.org/10.1144/GSL.SP.1990.051.01.25>

720   Murphy, J.B., Nance, R.D., 1989. Model for the evolution of the Avalonian-Cadomian belt.



721       Geology 17, 735–738. <https://doi.org/10.1130/0091->  
 722       7613(1989)017<0735:MFTEOT>2.3.CO;2  
 723   Nance, R.D., Murphy, J.B., 1994. Contrasting basement isotopic signatures and the palinspastic  
 724       restoration of peripheral orogens: Example from the Neoproterozoic Avalonian-Cadomia  
 725       belt. *Geology* 22, 617–620. <https://doi.org/10.1130/0091->  
 726       7613(1994)022<0617:CBISAT>2.3.CO;2  
 727   Nance, R.D., Murphy, J.B., 1996. Basement isotopic signatures and Neoproterozoic  
 728       paleogeography of Avalonian-Cadomian and related terranes in the circum-North Atlantic,  
 729       in: Nance, R.D., Thompson, M.D. (eds.), *Avalonian and Related Peri-Gondwanan Terranes*  
 730       of the Circum North Atlantic. Geological Society of America Special Paper 304, pp. 333–  
 731       346.  
 732   Pál-Molnár, E., Batki, A., Kiss, B., Upton, B.G.J., Markl, G., Odling, N., Harangi, S., 2015.  
 733       Origin of mafic and ultramafic cumulates from the Ditrău Alkaline Massif, Romania. *Lithos*  
 734       239, 1–18. <https://doi.org/10.1016/j.lithos.2015.09.022>  
 735   Pe-Piper, G., Piper, D.J.W., 2018. The Jeffers Brook diorite–granodiorite pluton: style of  
 736       emplacement and role of volatiles at various crustal levels in Avalonian appinites, Canadian  
 737       Appalachians. *International Journal of Earth Sciences* 107, 863–883.  
 738       <https://doi.org/10.1007/s00531-017-1536-z>  
 739   Pearce, J.A., 1983. Role of the Sub-continental Lithosphere in Magma Genesis at Active  
 740       Continental Margins, in: Hawkesworth, C.J., Norry, M. (eds.), *Continental Basalts and*  
 741       *Mantle Xenoliths*. Shiva Publications, Nantwich, Cheshire, pp. 230–249.  
 742   Pitcher, W.S., 1997. *The Nature and Origin of Granite*, 2nd ed. Chapman and Hall, London.  
 743   Pitcher, W.S., Berger, A.R., 1972. The Appinite suite: basic rocks genetically associated with

granite, in: *The Geology of Donegal. A Study of Granite Emplacement and Unroofing.*  
Regional Geology Series. John Wiley and Sons Ltd, Chichester, Sussex, pp. 143–168.

Pitcher, W.S., Hutton, D.H.W., 2003. *A Master Class Guide to the Granites of Donegal:*  
Geological Survey of Ireland. Geological Survey of Ireland.

Putirka, K., 2016. Amphibole thermometers and barometers for igneous systems and some  
implications for eruption mechanisms of felsic magmas at arc volcanoes. *American*  
*Mineralogist* 101, 841–858. <https://doi.org/10.2138/am-2016-5506>

Ridolfi, F., Renzulli, A., 2012. Calcic amphiboles in calc-alkaline and alkaline magmas:  
thermobarometric and chemometric empirical equations valid up to 1,130 °C and 2.2 GPa.  
*Contributions to Mineralogy and Petrology* 163, 877–895. [https://doi.org/10.1007/s00410-](https://doi.org/10.1007/s00410-011-0704-6)  
011-0704-6

Rock, N.M.S., 1990. *Lamprophyres.* Blackie, Glasgow.

Sato, M., 1978. Oxygen fugacity of basaltic magmas and the role of gas-forming elements.  
*Geophysical Research Letters* 5, 447–449. <https://doi.org/10.1029/GL005i006p00447>

Sharp, Z.D., 1990. A laser-based microanalytical method for the in situ determination of oxygen  
isotope ratios of silicates and oxides. *Geochimica et Cosmochimica Acta* 54, 1353–1357.  
[https://doi.org/10.1016/0016-7037\(90\)90160-M](https://doi.org/10.1016/0016-7037(90)90160-M)

Shaw, A.M., Hauri, E.H., Behn, M.D., Hilton, D.R., Macpherson, C.G., Sinton, J.M., 2012.  
Long-term preservation of slab signatures in the mantle inferred from hydrogen isotopes.  
*Nature Geoscience* 5, 224–228. <https://doi.org/10.1038/ngeo1406>

Shaw, A.M., Hauri, E.H., Fischer, T.P., Hilton, D.R., Kelley, K.A., 2008. Hydrogen isotopes in  
Mariana arc melt inclusions: Implications for subduction dehydration and the deep-Earth  
water cycle. *Earth and Planetary Science Letters* 275, 138–145.

767       <https://doi.org/10.1016/j.epsl.2008.08.015>  
 768   Sheppard, S.M.F., 1986a. Characterization and isotopic variations in natural waters, in: Valley,  
 769       J.W., Taylor, H.P., O'Neil, J.R. (eds.), *Stable Isotopes. Reviews in Mineralogy and*  
 770       *Geochemistry*, pp. 165–181.  
 771   Sheppard, S.M.F., 1986b. Igneous rocks; III, Isotopic case studies of magmatism in Africa,  
 772       Eurasia and oceanic islands, in: Valley, J.W., Taylor, H.P., O'Neil, J.R. (eds.), *Stable*  
 773       *Isotopes. Reviews in Mineralogy and Geochemistry*, pp. 319–371.  
 774   Sisson, Virginia B, Pavlis, Terry L, Roeske, Sarah M, Thorkelson, D.J., 2003. Introduction: An  
 775       overview of ridge-trench interactions in modern and ancient settings, in: Sisson, V.B.,  
 776       Roeske, S.M., Pavlis, T.L. (eds.), *Geology of a Transpressional Orogen Developed during*  
 777       *Ridge-Trench Interaction along the North Pacific Margin. Geological Society of America*  
 778       *Special Paper*, Boulder, Colorado, pp. 1–18. <https://doi.org/10.1130/0-8137-2371-X.1>  
 779   Sun, S.S., McDonough, W.F., 1989. Chemical and isotopic systematics of oceanic basalts:  
 780       Implications for mantle composition and processes, in: Saunders, A.D., Norry, M.J. (eds.),  
 781       *Magmatism in the Ocean Basins. Geological Society Special Publication*, pp. 313–345.  
 782       <https://doi.org/10.1144/GSL.SP.1989.042.01.19>  
 783   Suzuoki, T., Epstein, S., 1976. Hydrogen isotope fractionation between OH-bearing minerals and  
 784       water. *Geochimica et Cosmochimica Acta* 40, 1229–1240. [https://doi.org/10.1016/0016-](https://doi.org/10.1016/0016-7037(76)90158-7)  
 785       7037(76)90158-7  
 786   Taylor, B.E., Eichelberger, J.C., Westrich, H.R., 1983. Hydrogen isotopic evidence of rhyolitic  
 787       magma degassing during shallow intrusion and eruption. *Nature* 306, 541–545.  
 788       <https://doi.org/10.1038/306541a0>  
 789   Taylor, H.P., 1968. *The Oxygen Isotope Geochemistry of Igneous Rocks. Contributions to*

790 Mineralogy and Petrology 19, 1–71. <https://doi.org/10.1007/BF00371729>

791 Tiepolo, M., Tribuzio, R., Langone, A., 2011. High-Mg andesite petrogenesis by amphibole  
792 crystallization and ultramafic crust assimilation: Evidence from Adamello hornblendites  
793 (Central Alps, Italy). *Journal of Petrology* 52, 1011–1045.  
794 <https://doi.org/10.1093/petrology/egr016>

795 Ulrych, J., Krmíček, L., Teschner, C., Skála, R., Adamovič, J., Ďurišová, J., Křížová, Š.,  
796 Kuboušková, S., Radoň, M., 2018. Chemistry and Sr-Nd isotope signature of amphiboles of  
797 the magnesio-hastingsite–pargasite–kaersutite series in Cenozoic volcanic rocks: Insight  
798 into lithospheric mantle beneath the Bohemian Massif. *Lithos* 312–313, 308–321.  
799 <https://doi.org/10.1016/j.lithos.2018.05.017>

800 Valley, J.W., 2003. Oxygen Isotopes in Zircon. *Reviews in Mineralogy and Geochemistry* 53,  
801 343–385. <https://doi.org/10.2113/0530343>

802 Valley, J.W., Kinny, P.D., Schulze, D.J., Spicuzza, M.J., 1998. Zircon megacrysts from  
803 kimberlite: oxygen isotope variability among mantle melts. *Contributions to Mineralogy  
804 and Petrology* 133, 1–11. <https://doi.org/10.1007/s004100050432>

805 Valley, J.W., Lackey, J.S., Cavoie, A.J., Clechenko, C.C., Spicuzza, M.J., Basei, M.A.S.,  
806 Bindeman, I.N., Ferreira, V.P., Sial, A.N., King, E.M., Peck, W.H., Sinha, A.K., Wei, C.S.,  
807 2005. 4.4 billion years of crustal maturation: Oxygen isotope ratios of magmatic zircon.  
808 *Contributions to Mineralogy and Petrology* 150, 561–580. [https://doi.org/10.1007/s00410-](https://doi.org/10.1007/s00410-005-0025-8)  
809 [005-0025-8](https://doi.org/10.1007/s00410-005-0025-8)

810 Vennemann, T.W., O’Neil, J.R., 1996. Hydrogen isotope exchange reactions between hydrous  
811 minerals and molecular hydrogen: I. A new approach for the determination of hydrogen  
812 isotope fractionation at moderate temperatures. *Geochimica et Cosmochimica Acta* 60,

813 2437–2451. [https://doi.org/10.1016/0016-7037\(96\)00103-2](https://doi.org/10.1016/0016-7037(96)00103-2)

814 White, C.E., Barr, S.M., Hamilton, M.A., Murphy, J.B., 2021. Age and tectonic setting of  
815 Neoproterozoic granitoid rocks, Antigonish Highlands, Nova Scotia, Canada: Implications  
816 for Avalonia in the northern Appalachian orogen. *Canadian Journal of Earth Sciences* 59.  
817 <https://doi.org/https://doi.org/10.1139/cjes-2020-0110>

818 Wilkin, R.T., Bornhorst, T.J., 1993. Archean appinites from the Northern Complex, Michigan.  
819 *Journal of Geology* 101, 107–114. <https://doi.org/10.1086/648199>

820 Wolff, J.A., Balsley, S.D., Gregory, R.T., 2002. Oxygen isotope disequilibrium between quartz  
821 and sanidine from the Bandelier Tuff, New Mexico, consistent with a short residence time  
822 of phenocrysts in rhyolitic magma. *Journal of Volcanology and Geothermal Research*.  
823 [https://doi.org/10.1016/S0377-0273\(02\)00214-7](https://doi.org/10.1016/S0377-0273(02)00214-7)

824 Ye, H.M., Li, X.H., Li, Z.X., Zhang, C.L., 2008. Age and origin of high Ba-Sr appinite-granites  
825 at the northwestern margin of the Tibet Plateau: Implications for early Paleozoic tectonic  
826 evolution of the Western Kunlun orogenic belt. *Gondwana Research* 13, 126–138.  
827 <https://doi.org/10.1016/j.gr.2007.08.005>

828 Zheng, Y.-F., 1993. Calculation of oxygen isotope fractionation in magmatic rocks. *Chemical*  
829 *Geology* 120, 247–263. [https://doi.org/10.1016/0012-821X\(93\)90243-3](https://doi.org/10.1016/0012-821X(93)90243-3)

830

831

832

## Figure Captions

### Figure 1.

(a) Global reconstruction of Avalonia and Cadomia along the periphery of Gondwana (after Keppie et al., 1996; Nance and Murphy, 1996, 1994) showing subduction along the length of Avalonia and Cadomia with a transform fault. (b) Tectonic map of the northern Appalachian orogen (from Murphy et al., 2012 after Hibbard et al., 2007) with inset showing northern Antigonish Highlands, within the Avalon terrane (Avalonia) of Nova Scotia. CBI, Cape Breton Island; NB, New Brunswick; NE, New England; NL, Newfoundland; NS, Nova Scotia; QUE, Quebec. (c) Geological map of the northern Antigonish Highlands displaying the Greendale Complex between the Hollow and Greendale faults, intruding late Neoproterozoic Georgeville Group (from Murphy et al., 2012 after Murphy et al., 1997b). U-Pb data boxed (see text for details).

### Figure 2.

(a) Mixing and mingling of felsic, mafic and ultramafic appinite. Acicular hornblendes appear to co-precipitate with plagioclase. (b) Ultramafic layer intruded by a conjugate set of felsic veins. (c) Mafic porphyry displaying a “stacked log” linear fabric defined by amphibole oriented perpendicular to vein walls. Felsic veins cross-cut this sequence. (d) Acicular hornblende crystals in cross section displaying “salt and pepper” texture and co-precipitation with plagioclase.

### Figure 3.

(a) Hornblende (Hbl) from an ultramafic rock with inclusions of olivine (Ol) and serpentine (Srp), olivine has locally broken down to serpentine. (b) Ultramafic sample displaying poikilitic

hornblende enclosing olivine and clinopyroxene (Cpx). (c) Hornblende from an ultramafic sample showing mineral growth sequence with olivine enclosed by clinopyroxene which itself is enclosed by hornblende. (d) Hornblende from a mafic sample showing coprecipitation of hornblende and plagioclase (Pl). (e) Core of saussurite (Sst) with rim of fresh albite (Ab) in contact with hornblende in a mafic rock. (f) Hornblende from a felsic rock showing coprecipitation with plagioclase, extensive sericitisation of feldspathic matrix is visible.

Figure 4.

4-Fold Al apfu ( $Al^{IV}$ ) plotted against Al total apfu ( $Al^{tot}$ ) for amphiboles from mafic and ultramafic rocks (data from Murphy et al., 2012). Procedure for assigning Al according to Leake et al. (2004). Dashed line indicates composition of Edenite (Ed) and Tschermak (Ts) substitutions.

Figure 5.

Chondrite-normalized REE diagram for Group A and B amphiboles from ultramafic rocks (modified from Murphy et al. 2012). Chondrite normalized values from Sun and McDonough (1989).

Figure 6.

Histogram showing  $\delta^{18}O$  values for amphiboles from ultramafic, mafic and felsic rocks. Interpreted Group B and Group A ranges are shown above the histogram using data for mantle zones from Valley et al. (1998), zircon  $5.3 \pm 0.6$  ‰; Bindeman (2008), MORB  $5.7 \pm 0.2$  ‰;

878 Chazot et al. (1997), amphibole 5.3–5.6 ‰, and associated supracrustal zones from Valley et al.  
879 (2005), > 5.9 ‰. Group A range interpreted from Bindeman (2008).

880

881 Figure 7.

882 Histogram showing  $\delta D$  values for amphiboles from ultramafic, mafic and felsic rocks.

883

884 Figure 8.

885 (a)  $Fe_{tot}$  a.p.f.u. (atoms per formula unit; from Murphy et al., 2012) versus  $\delta D$ . No correlation  
886 between these two parameters is visible. (b) Calculated  $Fe^{3+}/Fe^{2+}$  ratios (from Murphy et al.,  
887 2012) versus  $\delta D$  values for amphiboles from mafic and ultramafic rocks. A weak inverse  
888 correlation is visible.

889

890 Figure 9.

891 (a) Calculated  $\delta D_{fluid}-\delta^{18}O_{fluid}$  plot of amphibole fluid source from ultramafic, mafic and felsic  
892 rocks. Fields for organic, metamorphic and primary magmatic waters are from Sheppard  
893 (1986a).  $\delta D_{fluid}$  is calculated using fractionation equation from Graham et al. (1984).  $\delta^{18}O_{fluid}$  is  
894 calculated using fractionation equation from Zheng (1993). Both calculations are made for a  
895 temperature estimate of 700 °C. (b) Calculated  $\delta D_{fluid}-\delta^{18}O_{fluid}$  plot of amphibole fluid source  
896 from ultramafic, mafic and felsic rocks. Fields for organic, metamorphic and primary magmatic  
897 waters are from Sheppard (1986a).  $\delta D_{fluid}$  is calculated using fractionation equation from  
898 Suzuoki & Epstein (1976).  $\delta^{18}O_{fluid}$  is calculated using fractionation equation from (Zheng,  
899 1993). Both calculations are made for a temperature estimate of 700 °C.

900



Figure 10.

(a) 4-Fold Al apfu ( $Al^{IV}$ ) plotted against Al total apfu ( $Al^{tot}$ ) for amphiboles from mafic and ultramafic rocks (data from Murphy et al., 2012). Procedure for assigning Al according to Leake et al. (2004). Pressure estimates for 650 °C and 750 °C calculated using Anderson & Smith (1995). (b)  $Al_2O_3$  (wt. % from Murphy et al., 2012) plotted against pressure estimates, technique from Pál-Molnár et al. (2015). Laser ablation sample sites listed on x-axis. PG4, PG12, PG6, PG11, PG1 refer to amphiboles from ultramafic rocks. GR8-M, GR15-M, GR10-M and GR9-M refer to amphiboles from mafic rocks samples.

Figure 11.

(a) Calculated  $\delta D_{fluid-H_2O}$  (wt. %) plot showing progressive hydration trend of amphiboles from ultramafic, mafic and felsic rocks.  $\delta D_{fluid}$  is calculated using fractionation equation from Graham et al. (1984) at 700 °C. (b) Calculated  $\delta D_{fluid-H_2O}$  (wt. %) plot showing progressive hydration trend of amphiboles from ultramafic, mafic and felsic rocks.  $\delta D_{fluid}$  is calculated using fractionation equation from Suzuoki & Epstein (1976) at 700 °C.

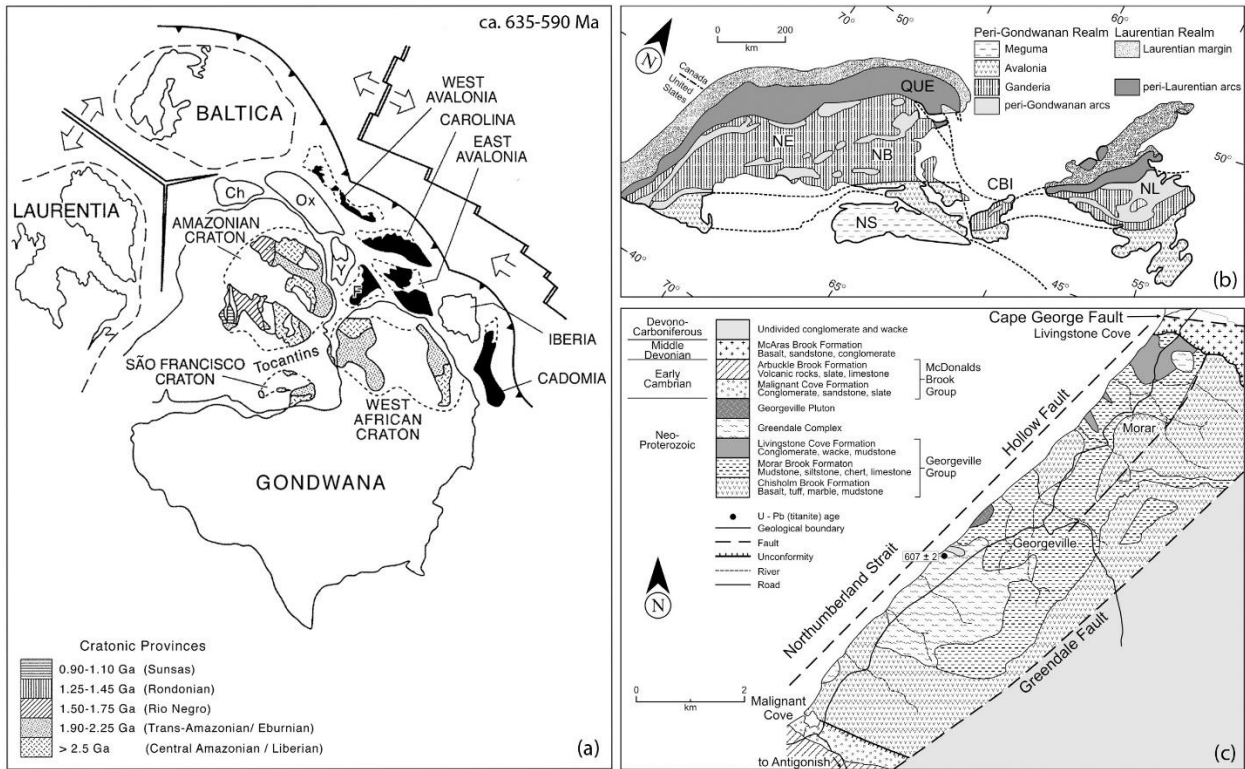
Figure 12.

Conceptual model showing the development of a slab window by ridge-trench interaction (modified from Murphy, 2020 after Sisson et al., 2003). Note location of Greendale Complex next to Hollow-Greendale fault and association with Antigonish Granites and other felsic magmas. Detail on right (modified from Murphy, 2020) shows progressive ascent of magma next to Hollow-Greendale fault. Symbols indicate throw on Hollow-Greendale fault system. 1) dissolved mantle water in magma system, 2) crystallization of Group B hornblende with mantle

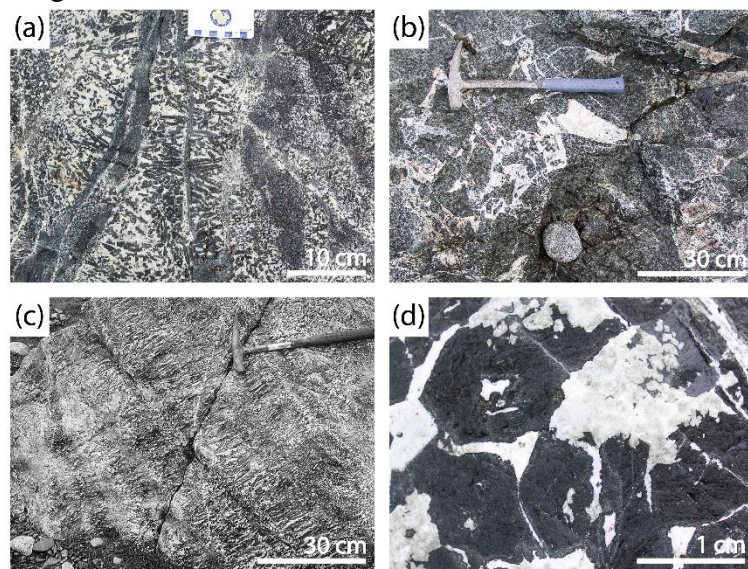
derived fluids, 3) shallow crust crystallization of Group A hornblende with mixed water sources including assimilation of earlier hydrothermally altered phases. Progressive ascent of magma system results in re-equilibration of Group B hornblende following the assimilation of supracrustal sedimentary and volcanic rocks. Felsic magmas form by fractionation of a mafic parent, by anatexis (hydrous melting) of the lower crust as shown by Sm-Nd data from Murphy & Dostal (2007). They rise to the mid- and upper-crust and form a rheological barrier to the subsequent ascent of mafic magma. Early mafic intrusions are entrained as enclaves so that only the appinites at the extremities of the system are preserved intact.

# Figures

Figure 1.

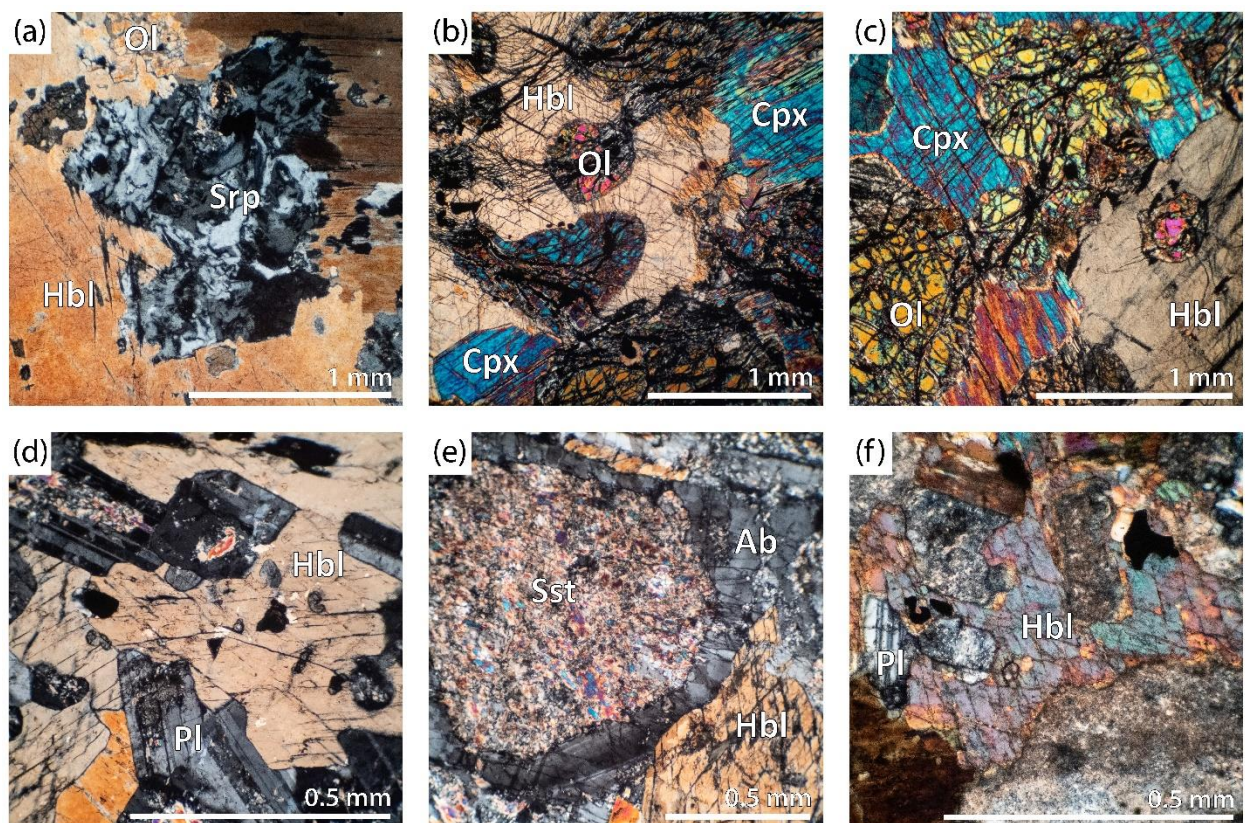


937 Figure 2.



938

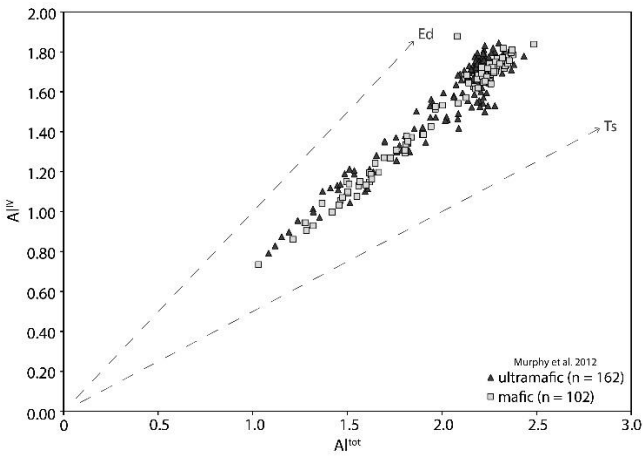
939 Figure 3.



940

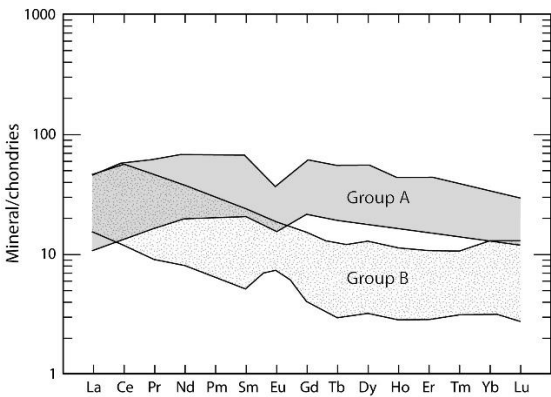
941

942 Figure 4.



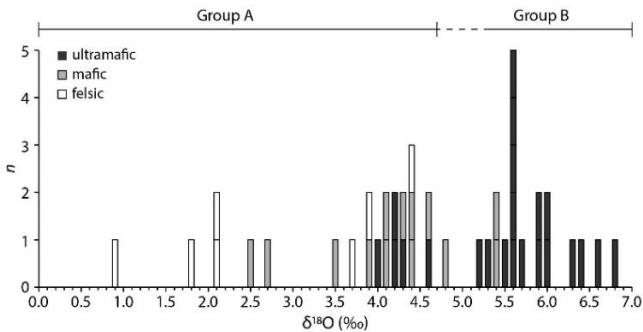
943

944 Figure 5.



947

948 Figure 6.



949

950

951 Figure 7.



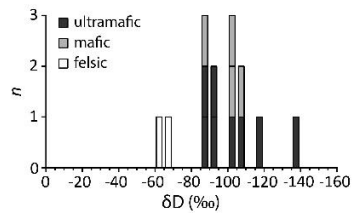


Figure 8.

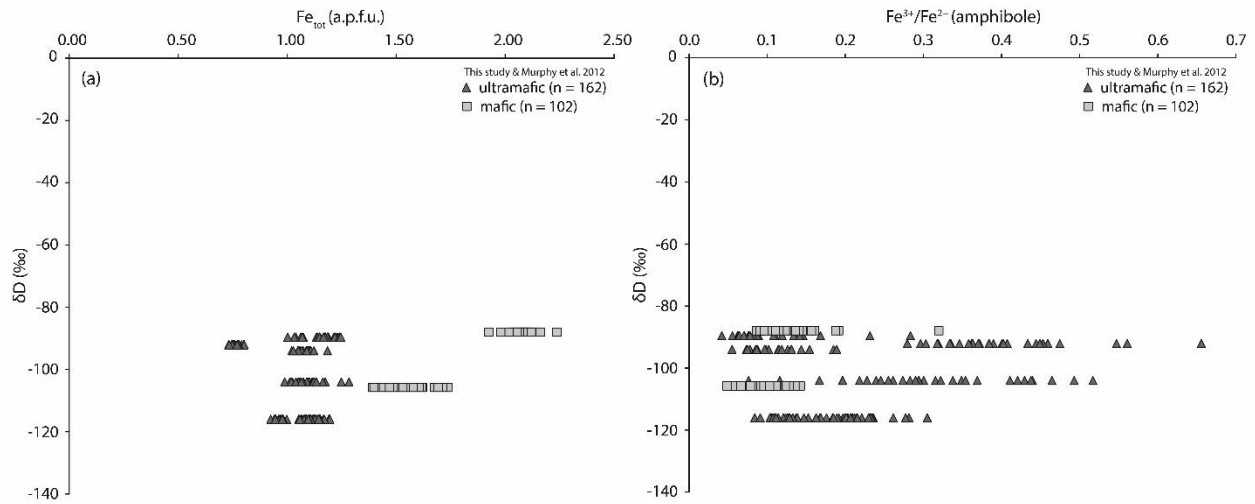
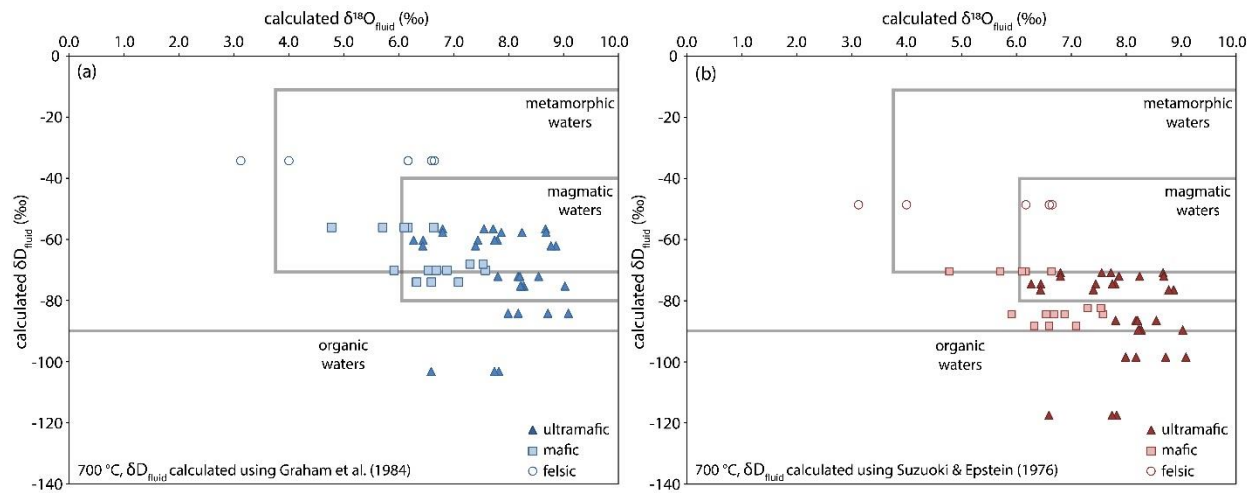
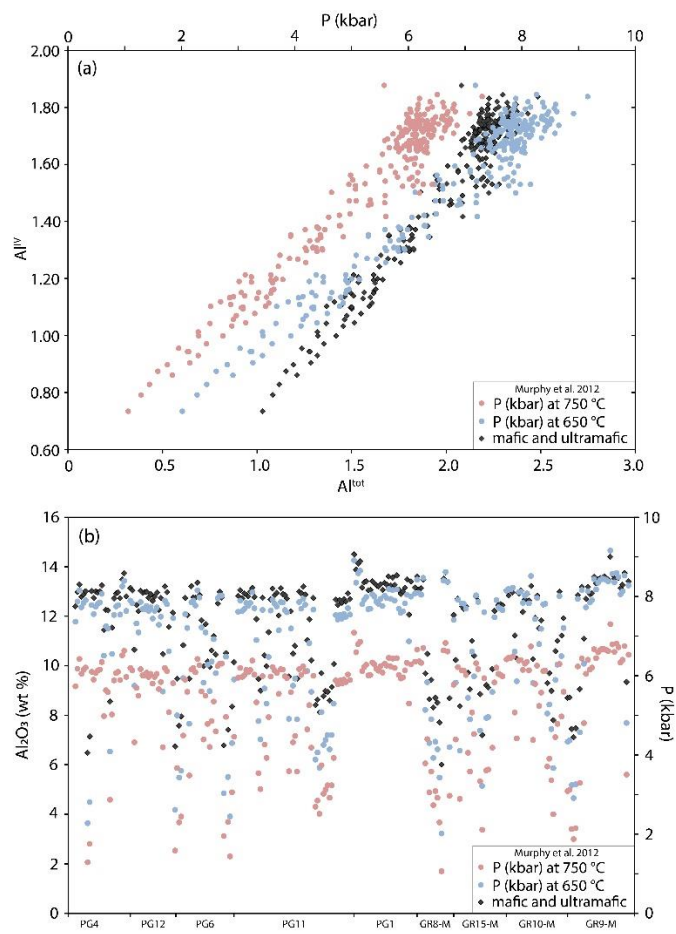


Figure 9.



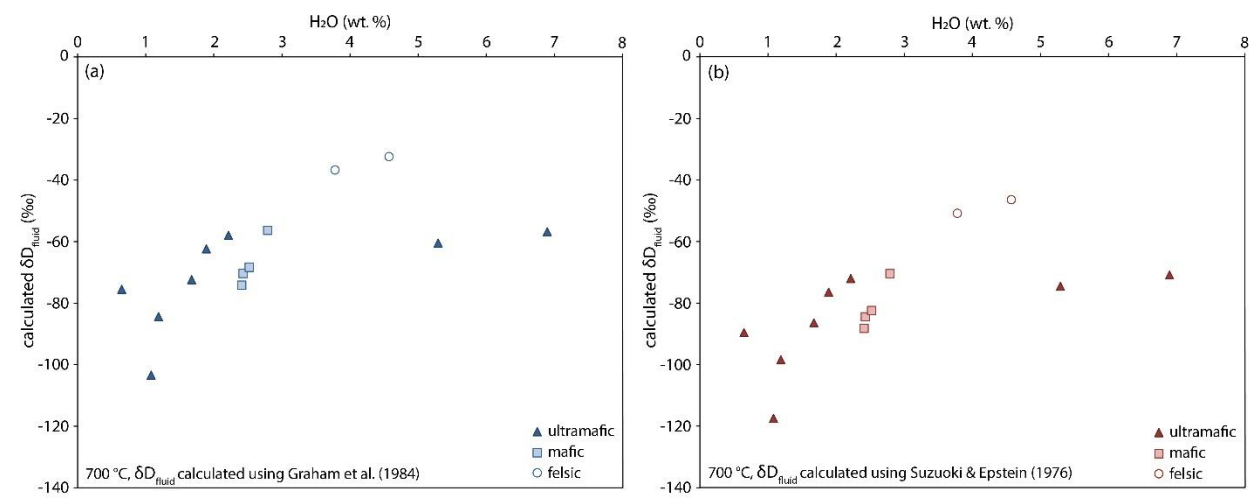
960 Figure 10.



961

962

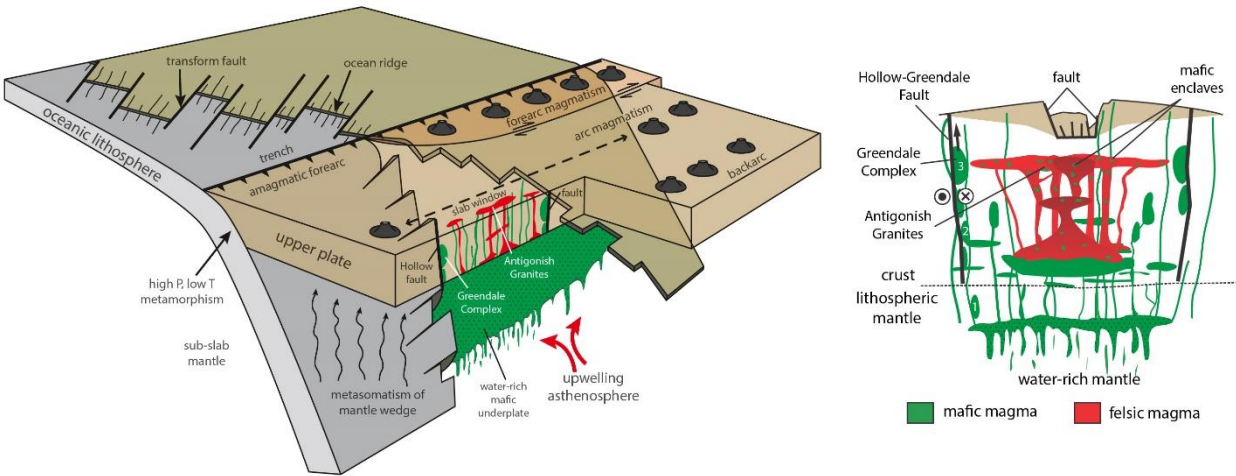
963 Figure 11.



964

965

966 Figure 12.



967

968

969

970    **Table captions**

971    Table 1.  $\delta^{18}\text{O}$  of drilled amphibole and single mineral separates from Greendale Complex  
972    lithologies (‰ V-SMOW).  $\delta^{18}\text{O}$  water is calculated using the equations of Zheng (1993) at a  
973    temperature average of 700 °C.

974

975    Table 2.  $\delta\text{D}$  of single mineral separates from Greendale Complex lithologies (‰ V-SMOW).  $\delta\text{D}$   
976    water<sup>a</sup> is calculated using the equations of Graham et al. (1984) and  $\delta\text{D}$  water<sup>b</sup> is calculated using  
977    the equations of Suzuoki & Epstein (1976), both calculations use a temperature average of  
978    700 °C.



979 **Tables**

980 Table 1

Sample	Unit	$\delta^{18}\text{O}$ amphibole (‰ V-SMOW)	$\delta^{18}\text{O}$ water (‰ V-SMOW) T 700 °C	Average $\delta^{18}\text{O}$ amphibole (‰ V-SMOW)	$\sigma$
PG1-A	ultramafic	4.2	6.4	4.9	0.7
PG1-B		5.6	7.8		
PG1-C		5.2	7.4		
PG1-D		5.5	7.8		
PG1-X		4.0	6.3		
PG2-A*	ultramafic	6.4	8.7	5.4	0.8
PG2-B*		5.5	7.7		
PG2-C*		5.3	7.6		
PG2-X*		4.6	6.8		
PG4-A	ultramafic	6.0	8.2	5.7	0.8
PG4-B		4.6	6.8		
PG4-C		5.6	7.9		
PG4-X		6.4	8.7		
PG5-A*	ultramafic	6.8	9.0	6.2	0.4
PG5-B*		6.0	8.3		
PG5-C*		6.0	8.2		
PG5-X*		6.0	8.2		
PG6-A	ultramafic	5.6	7.8	5.9	0.3
PG6-B		6.3	8.6		
PG6-C		5.9	8.2		
PG6-X		6.0	8.2		
PG7-A	ultramafic	5.6	7.8	5.3	0.7
PG7-B		4.3	6.6		
PG7-C		5.6	7.8		
PG7-X		5.5	7.7		
PG11-A	ultramafic	5.9	8.2	6.2	0.5
PG11-C		6.8	9.1		
PG11-D*		6.5	8.7		
PG11-X		5.7	8.0		
PG12-A	ultramafic	4.2	6.4	5.6	1.2
PG12-B		6.6	8.9		
PG12-C		5.2	7.4		
PG12-X2*		6.5	8.8		
GR9-M-A	mafic	4.1	6.3	4.3	0.4
GR9-M-B		2.7	5.0		
GR9-M-C		4.4	6.6		
GR9-M-D		4.8	7.1		
GR9-M-E*		2.1	4.4		
GR9-M-X		4.1	6.3		
GR15-M-A	mafic	2.5	4.8	3.6	0.7
GR15-M-B		3.5	5.7		
GR15-M-D		3.9	6.2		
GR15-M-E*		4.4	6.6		
GR15-M-X		3.9	6.1		
GX1-A	mafic	4.3	6.5	4.5	0.6
GX1-B		4.4	6.7		
GX1-C		4.6	6.9		
GX1-D		3.7	5.9		
GX1-X		5.3	7.6		
GX2-X	mafic	5.3	7.5	5.2	0.2
GX2-X2*		5.1	7.3		
GR8-F-A	felsic	2.1	4.4	2.1	
GR9-F-A	felsic	2.1	4.3	2.1	
GR5-F-A	felsic	0.9	3.1	3.1	1.6
GR5-F-B		1.8	4.0		
GR5-F-C		3.9	6.2		
GR5-F-E*		4.4	6.6		
GR5-F-X		4.4	6.7		

981

\* Indicates use of second standard set (2019 samples) YP2, GP147 and UWG2. Labels without \* indicate initial sample set (2017 samples) using TOR1, YP2, SCXO, JJB8 and GP147 standards.

Table 2

Sample	Unit	$\delta D$ amphibole (‰ V-SMOW)	$\delta D$ water <sup>a</sup> (‰ V-SMOW) T 700 °C	$\delta D$ water <sup>b</sup> (‰ V-SMOW) T 700 °C
PG1	ultramafic	-92	-60	-75
PG2	ultramafic	-88	-57	-71
PG4	ultramafic	-90	-58	-72
PG5	ultramafic	-107	-75	-90
PG6	ultramafic	-104	-72	-87
PG7	ultramafic	-135	-103	-118
PG11	ultramafic	-116	-84	-99
PG12	ultramafic	-94	-62	-77
GR9-M	mafic	-106	-74	-88
GR15-M	mafic	-88	-56	-71
GX1	mafic	-102	-70	-85
GX2	mafic	-100	-68	-82
GR5-F	felsic	-64	-32	-47
		-68	-37	-51